



OPEN Research on leakage and diffusion behavior of hydrogen doped natural gas in integrated pipeline corridors based on data drive

Xiaolong Gong¹, Hua Li¹, Cheng Li¹, Mingyue Kou^{2✉}, Lingxu Kong^{1,3} & Hongcheng Liu^{1,3}

With the wide application of hydrogen-doped natural gas (HBNG) in end users, laying pipelines in urban, comprehensive pipe corridors has become increasingly common. However, the leakage and diffusion of hydrogen-doped natural gas in confined or semi-confined spaces (e.g., utility corridors) can pose a severe safety hazard, as methane and hydrogen gas mixtures have a higher risk of explosion. Therefore, studying hydrogen-doped natural gas's leakage and diffusion behavior in the comprehensive pipe gallery is essential to ensure its safe operation. This paper establishes a numerical model to study the diffusion law of hydrogen-doped natural gas leakage, and the concentration distribution under different conditions is analyzed. The evolution of the leakage and diffusion of hydrogen-doped natural gas under different hydrogen doping ratios, wind speeds, inlet and outlet spacing, and leakage port sizes were simulated, and the effects of these factors on gas diffusion and explosion hazard volume were discussed. In addition, the backpropagation neural network (BPNN) combined with the global optimization capability of genetic algorithm and the nonlinear mapping capability of neural network is used in this paper to provide a reliable technical means for the accurate prediction of explosion risk volume, which has important application value in the safety design of pipeline corridor and accident prevention and control. The results show that the diffusion range of gas in the pipe corridor increases significantly with the increase of hydrogen mixing ratio. When the hydrogen mixing ratio decreases from 20% to 0, the explosion volume of CH₄ decreases by 12.25%. The explosion volume of H₂ is close to 0. At the same time, the greater the distance between inlet and outlet, the wider the spread of the dangerous area, when the distance between inlet and outlet is reduced from 200 m to 100 m, the explosion volume of CH₄ is reduced by 99.92%, and the explosion volume of H₂ is reduced by 100%. In the case of emergency, the reasonable design of Distance between inlet and outlet and air flow configuration can help to quickly discharge harmful gases, ensure the safe evacuation and equipment maintenance in the pipe corridor, and have guiding significance for the ventilation design of the pipe corridor.

Keywords Hydrogen-blended natural gas, Leakage diffusion, Utility tunnel, Backpropagation neural network

In view of the great potential of hydrogen in energy transformation and sustainable development around the world, how to realize the adequate transportation of hydrogen has become a hot spot of concern¹. Among them, as a critical form of hydrogen transportation, natural gas hydrogen mixing technology is developing rapidly. Meanwhile, as a new type of pipeline (hydropower, gas, etc.) laying method is necessary for developing civilized cities, the construction of underground pipe galleries is also in full swing. The two's rapid growth and application overlap will inevitably lead to many hydrogen-doped natural gas pipelines passing through the underground pipe gallery to deliver hydrogen to end users. According to statistics, large-scale natural gas pipelines are currently laid in the underground pipe gallery. It is worth noting that the change in the conveying medium will inevitably lead to a difference in the fluid dynamics performance of the leakage and diffusion behavior of the medium and further affect the response of the relevant safety control measures²⁻⁵. Therefore, exploring the leakage and diffusion characteristics of hydrogen-doped natural gas pipelines in the underground pipe gallery can enhance

¹Northwest Sichuan Gas District of Southwest Oil and Gasfield Company, Jiangyou 621700, China. ²College of Petroleum and Natural Gas Engineering, SouthWest Petroleum University, Chengdu 610500, China. ³Lingxu Kong and Hongcheng Liu contributed equally to this work. ✉email: 18381029336@163.com

the understanding of safety management and control and help to further promote the development of energy transformation and low-carbon society.

Methane and hydrogen leakage, diffusion, and explosion in confined or semi-confined environments have been the subject of numerous investigations by domestic and international researchers. When the hydrogen blending ratio was less than 50%, the accumulation behavior of hydrogen-doped natural gas was comparable to that of pure natural gas, according to Lowesmith's⁶ study on the leakage and accumulation behavior of hydrogen-doped natural gas in confined areas. Wilkening et al.⁷ simulated the diffusion and leakage of pure methane and H₂-CH₄ mixture gas in the pipeline under windy and windless conditions, respectively, and discovered that the mixed gas's leakage rate and volume were greater than methane's. The research of Li Du⁸ and Li Ranran et al.⁹ showed that the static storage of hydrogen-doped natural gas after leakage in the kitchen would cause gas stratification, and different gas components and leakage conditions had significant effects on the concentration distribution. In order to examine the diffusion law and leakage of hydrogen-doped natural gas in a valve chamber under various hydrogen volume concentrations, wind speeds, leakage diameters, and leakage port directions, Jia Wenlong et al.¹⁰ used a typical valve chamber from the West-East Gas Pipeline as an example. Stefano¹¹ and Mohammad et al.¹² studied how the diffusion of hydrogen in a confined space is significantly affected by the leak rate, while the leak location is less affected, and revealed the diffusion behavior of the gas and measured the danger height and vanishing moment. Gupta et al.¹³'s research shows that the peak concentration of helium leakage in a closed garage is mainly determined by the total amount of leakage, while the leakage rate affects the gas mixing behavior. In addition, Jiang, H et al.¹⁴ based on the case of "6.13" explosion accident in Shiyan City, Hubei Province, calculated the amount of natural gas involved from three perspectives: TNT equivalent of explosion energy, damage to buildings and overpressure distribution in buildings.

Some scholars have conducted relevant studies on the gas leakage and diffusion of public pipe corridors. From the perspective of gas leakage and diffusion characteristics, Lei Peng et al.¹⁵ studied the diffusion of hydrogen leakage in the pipe gallery and found that the contact time after gas injection was long, resulting in slow propagation speed. Zhou Ning et al.¹⁶ simulated the diffusion process of natural gas in an underground pipeline corridor and found that under the action of wind, natural gas diffused in a "snail" shape and the turbulence intensity increased. From the perspective of leakage influencing factors, Duan Pengfei et al.¹⁷⁻¹⁸ studied the influence of leakage hole direction, diameter and hydrogen mixing ratio on natural gas concentration distribution. Sun et al.¹⁹ found that higher pipeline pressure increases the amount of gas leaking and accelerates the injection rate, leading to concentration stratification. Li Jingtao et al.²⁰ found that increased slope would shorten the alarm response time. Zhang Chenglong et al.²¹ analyzed the influence of multi-factor coupling on leakage and simulated leakage scenario. From the perspective of alarm and safety, Some scholars analyzed the process of leakage alarm and accident ventilation in the pipe gallery from the Angle of alarm and safety, and put forward the alarm scheme^{18,22}.

However, the leakage and diffusion of hydrogen-doped natural gas at home and abroad rarely consider the leakage of long and narrow underground structures such as pipe corridors. In addition, the current study mainly analyzes the gas leakage and diffusion behavior under fixed ventilation frequency and inlet and outlet spacing, and neural network prediction is less applied in this area, and more work needs to be done to fill these gaps. Therefore, a numerical model of leakage and diffusion of hydrogen-doped natural gas in the integrated pipeline corridor is established in this paper, and the difference of concentration distribution and velocity field of hydrogen-doped natural gas is analyzed under the conditions of different inlet speed, inlet and outlet spacing, hydrogen ratio and leakage port size. The explosion risk volume of methane and hydrogen under different conditions is predicted by backpropagation neural network. GA-BPANN can accurately model complex nonlinear relationships and process high-dimensional data. This method can be used for rapid and flexible risk assessment under various conditions, and can provide reliable information for safety design. It can influence the ventilation design of pipeline corridors, the layout design of hydrogen-doped natural gas pipelines, and the formulation of emergency repair strategies for pipeline corridors. The technical route is shown in Fig. 1.

Theory and methodology

Computational fluid theory

Control equations

The leakage and diffusion of gas in the pipe gallery first satisfies the law of conservation of mass²³. the continuous equation of gas leakage and diffusion in the pipe gallery is shown in Eq. (1).

$$\frac{\partial \rho}{\partial t} + \frac{\partial(\rho u_x)}{\partial x} + \frac{\partial(\rho u_y)}{\partial y} + \frac{\partial(\rho u_z)}{\partial z} = 0 \quad (1)$$

Where, ρ is the gas density (kg/m³). u is the velocity field of fluid (m/s).

The leakage and diffusion of hydrogen-doped natural gas in the pipe gallery must satisfy the law of conservation of energy²⁴, and its energy equation is shown in Eq. (2).

$$\frac{\partial(\rho h)}{\partial t} + \frac{\partial(\rho u_x h)}{\partial x} + \frac{\partial(\rho u_y h)}{\partial y} + \frac{\partial(\rho u_z h)}{\partial z} = -p \left(\frac{\partial u_x}{\partial x} + \frac{\partial u_y}{\partial y} + \frac{\partial u_z}{\partial z} \right) + \text{div}(\lambda \text{grad}T) + \phi + S_h \quad (2)$$

Where, h is the enthalpy of hydrogen-doped natural gas (J/mol), λ is the thermal conductivity (W·m⁻¹·K⁻¹), T is the thermodynamic temperature of the micro-element (K), ϕ is the energy dissipation function, S_h is the internal heat source term of the micro-element.

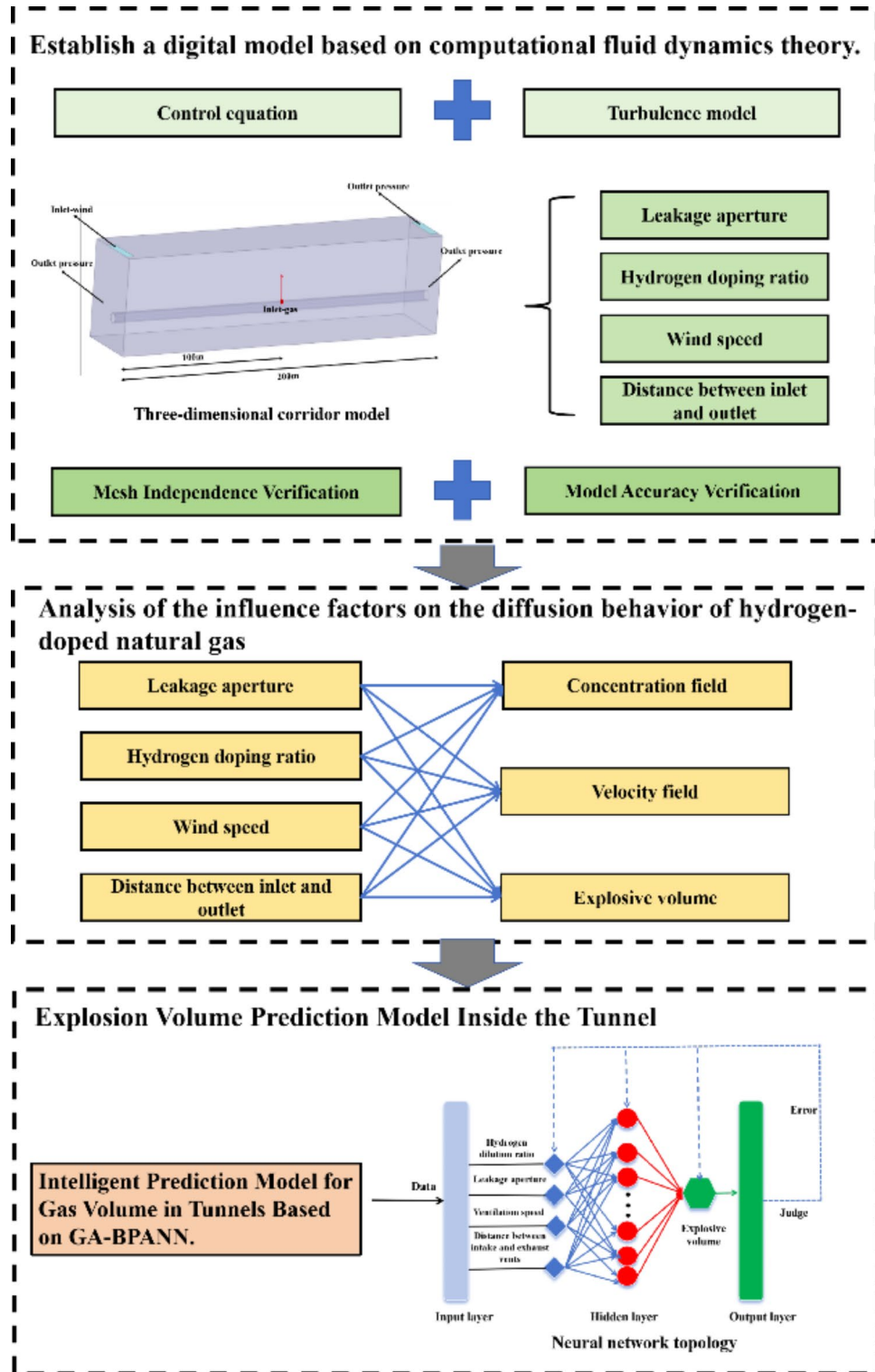


Fig. 1. Technology roadmap.

The momentum equation is describing the relationship between hydrogen-doped natural gas leakage and diffusion and air²⁵. The differential form is shown in Eq. (3), (4), (5).

$$\frac{\partial(\rho u_x)}{\partial t} + \frac{\partial(\rho u_x u_x)}{\partial x} + \frac{\partial(\rho u_x u_y)}{\partial y} + \frac{\partial(\rho u_x u_z)}{\partial z} = -\frac{\partial P}{\partial x} + \mu \left[\frac{\partial^2 u_x}{\partial x^2} + \frac{\partial^2 u_x}{\partial y^2} + \frac{\partial^2 u_x}{\partial z^2} \right] + F_x \quad (3)$$

$$\frac{\partial(\rho u_y)}{\partial t} + \frac{\partial(\rho u_x u_y)}{\partial x} + \frac{\partial(\rho u_y u_y)}{\partial y} + \frac{\partial(\rho u_y u_z)}{\partial z} = -\frac{\partial P}{\partial y} + \mu \left[\frac{\partial^2 u_y}{\partial x^2} + \frac{\partial^2 u_y}{\partial y^2} + \frac{\partial^2 u_y}{\partial z^2} \right] + F_y \quad (4)$$

$$\frac{\partial(\rho u_z)}{\partial t} + \frac{\partial(\rho u_x u_z)}{\partial x} + \frac{\partial(\rho u_y u_z)}{\partial y} + \frac{\partial(\rho u_z u_z)}{\partial z} = -\frac{\partial P}{\partial z} + \mu \left[\frac{\partial^2 u_z}{\partial x^2} + \frac{\partial^2 u_z}{\partial y^2} + \frac{\partial^2 u_z}{\partial z^2} \right] + F_z \quad (5)$$

where, μ is the dynamic viscosity ($\text{N}\cdot\text{s}/\text{m}^2$), F_x , F_y , F_z is the volume force (N) acting on the x , y , z coordinate axes by the infinitesimal body.

Component transmission equation

After the leakage and diffusion of hydrogen-doped natural gas pipeline in the pipe gallery, it will continuously blend with the air in the pipe gallery, which belongs to the blending and transmission of different components²⁶. There is no chemical reaction in this process, so the component transmission equation is equation (6).

$$\frac{\partial(\rho\omega)}{\partial t} + \frac{\partial(\rho u_x \omega)}{\partial x} + \frac{\partial(\rho u_y \omega)}{\partial y} + \frac{\partial(\rho u_z \omega)}{\partial z} = \frac{\partial}{\partial x} \left(\rho D_t \frac{\partial \omega}{\partial x} \right) + \frac{\partial}{\partial y} \left(\rho D_t \frac{\partial \omega}{\partial y} \right) + \frac{\partial}{\partial z} \left(\rho D_t \frac{\partial \omega}{\partial z} \right) \quad (6)$$

Where, ω is the mass fraction of the component, D_t is the turbulent diffusion coefficient (m^2/s).

Turbulence modeling

The Realizable k - ε turbulence model is used to represent the turbulent motion based on the features of the hydrogen-doped natural gas jet. Compared with the standard k - ε model, the realizable k - ε model shows substantial improvement, mainly in the case of flow field including strong streamline curvature, eddy current and rotation. The model is capable of accurately simulating gas leakage and diffusion processes, turbulent flow, jet flow, and mixed flow^{27,30}. This model's equation can be found in (7) and (8)³¹.

$$\begin{aligned} \frac{\partial}{\partial t} (\rho k) + \frac{\partial}{\partial x} (\rho k u_x) + \frac{\partial}{\partial y} (\rho k u_y) + \frac{\partial}{\partial z} (\rho k u_z) = \\ \frac{\partial}{\partial x} \left[\left(\mu + \frac{\mu_t}{\sigma_k} \right) \frac{\partial k}{\partial x} \right] + \frac{\partial}{\partial y} \left[\left(\mu + \frac{\mu_t}{\sigma_k} \right) \frac{\partial k}{\partial y} \right] + \frac{\partial}{\partial z} \left[\left(\mu + \frac{\mu_t}{\sigma_k} \right) \frac{\partial k}{\partial z} \right] + G_k + G_b - \rho \varepsilon - Y_M + S_k \end{aligned} \quad (7)$$

$$\begin{aligned} \frac{\partial}{\partial t} (\rho \varepsilon) + \frac{\partial}{\partial x} (\rho \varepsilon u_x) + \frac{\partial}{\partial y} (\rho \varepsilon u_y) + \frac{\partial}{\partial z} (\rho \varepsilon u_z) = \\ \frac{\partial}{\partial x} \left[\left(\mu + \frac{\mu_t}{\sigma_\varepsilon} \right) \frac{\partial \varepsilon}{\partial x} \right] + \frac{\partial}{\partial y} \left[\left(\mu + \frac{\mu_t}{\sigma_\varepsilon} \right) \frac{\partial \varepsilon}{\partial y} \right] + \frac{\partial}{\partial z} \left[\left(\mu + \frac{\mu_t}{\sigma_\varepsilon} \right) \frac{\partial \varepsilon}{\partial z} \right] + \rho C_1 S \varepsilon - \rho C_2 \frac{\varepsilon^2}{k + \sqrt{v \varepsilon}} + C_{1\varepsilon} \frac{\varepsilon}{k} C_{3\varepsilon} G_b + S_\varepsilon \end{aligned} \quad (8)$$

Where, k is the turbulent kinetic energy, ε is the turbulent dissipation rate, μ_t is the turbulent viscosity, G_k the turbulent kinetic energy generated by the average velocity gradient, G_b is the turbulent kinetic energy generated by the buoyancy effect, Y_M is the turbulent dissipation rate generated by the compression of the turbulent pulsation expansion, S_k and S_ε is the custom source term, $C_{1\varepsilon}=1.44$, $C_2=1.9$, $C_{3\varepsilon}$, $\sigma_\varepsilon=1.0$ and $\sigma_k=1.2$ are the model coefficients. $C_1 = \max \left[0.43, \frac{\eta}{\eta+5} \right]; \eta = S_{ij}^k; S = \sqrt{2S_{ij}S_{ij}}$.

Numerical model

Physical modeling and meshing

in order to comprehend the concentration distribution and diffusion behavior of hydrogen-doped natural gas in the public pipe gallery following leaking. As seen in Fig. 2(a), a three-dimensional physical model of the gas chamber of a $200 \text{ m} \times 1.8 \text{ m} \times 2.4 \text{ m}$ common pipe gallery was built. The installation spacing of pipes in the independent cabin of the public works pipe gallery is described in Fig. 2(b) in accordance with the Chinese national standard GB 50,838 – 2015 “Technical Code for Urban Comprehensive Pipe Corridor Engineering”³² and the pipe gallery is 1.8 m wide and 2.4 m high. The seamless steel pipe used for the hydrogen-doped natural gas pipeline has DN250, 400 mm a, 500 mm, and 800 mm for b_1 and b_2 , respectively. Considering the current state of engineering design, The air inlet and outlet have the same dimensions (1 m by 1 m). The pipe gallery is reduced to a long, narrow, rectangular building that has ventilatable walls on the left and right sides. The hydrogen-doped natural gas pipeline has a leak hole in the middle of its upper surface. The model mainly simulates the diffusion of hydrogen-doped natural gas in the pipe gallery after leakage into the atmosphere from small holes and analyzes the effects of ventilation velocity, inlet and outlet spacing, hydrogen blending ratio, and leakage port size on the diffusion of hydrogen-doped natural gas. Combined with several features of the model, a hexahedral mesh-based meshing strategy was adopted. The grid encryption grid is set up at the air inlet, outlet, and leak hole for locations prone to large velocity gradients, as shown in Fig. 2(c).

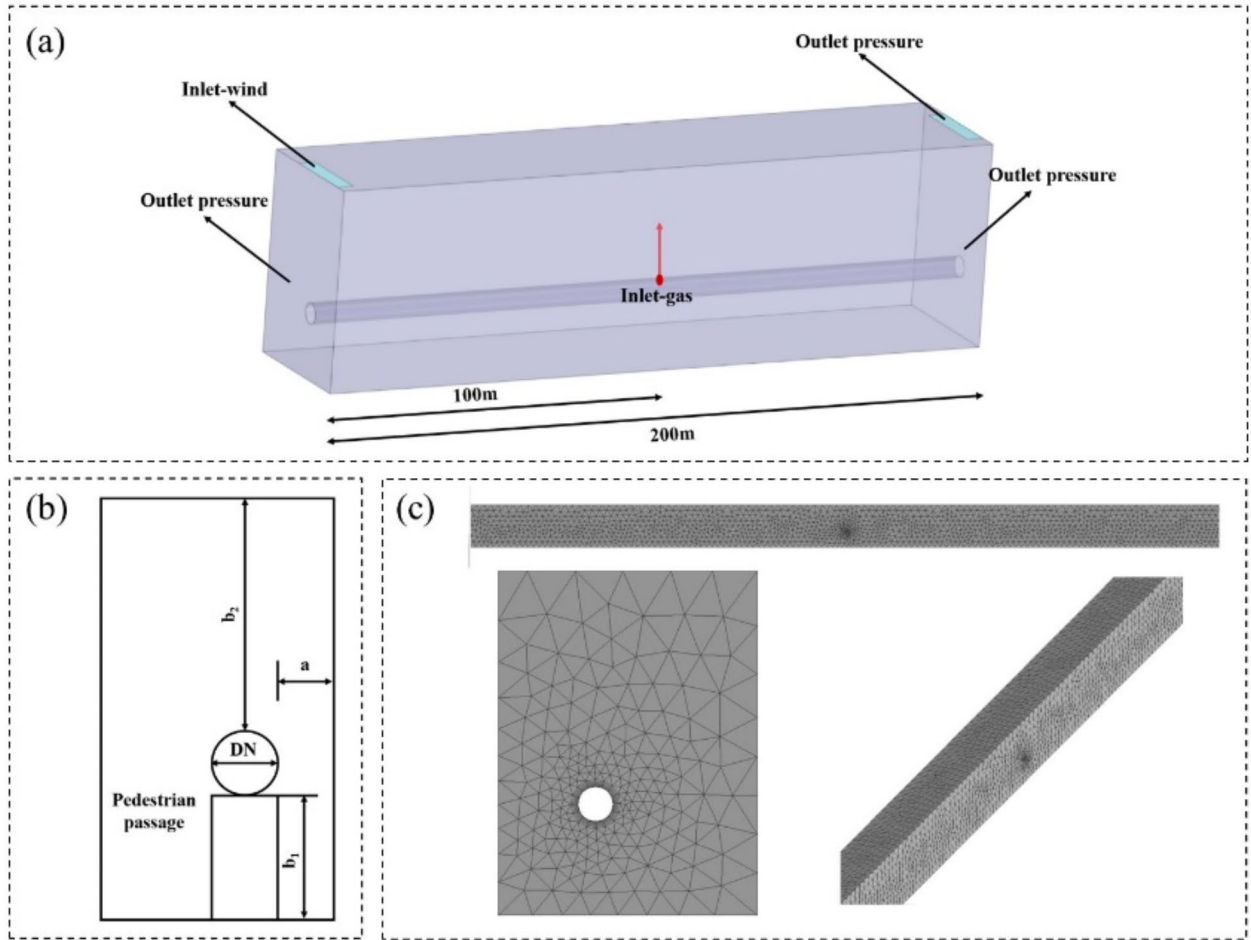


Fig. 2. Numerical model: (a) 3D pipe gallery model, (b) installation spacing of pipes in pipe gallery, (c) mesh generation strategy.

Category	Factor	数值
Piping design factors	Leak aperture size (mm)	10/20/30/40
	Hydrogen-doped ratio (%)	0/5/10/15/20
Ventilation conditions	Wind speed (m/s)	1.4/1.9/2.4/2.9
	Distance between air inlet and outlet (m)	50/100/150/200

Table 1. Classification and values of influencing factors.

Study of the design of working conditions

This paper, based on the “Technical Specifications for Urban Comprehensive Pipe Tunnel Engineering,” explores the effects of pipe body factors and ventilation conditions on the diffusion behavior of hydrogen-contaminated natural gas leaks³³. The selected influencing factors are listed in Table 1. According to the influencing factors, specific scenarios were designed as shown in Table 2.

Calculation of working condition parameters

Physical properties of gas mixtures The thermodynamic properties of the mixture gas can be calculated based on the gas mixture rules.

$$m = x_1m_1 + x_2m_2 + x_3m_3 + \dots + x_nm_n \tag{9}$$

$$c_{p,m} = x_1c_{p,1} + x_2c_{p,2} + x_3c_{p,3} + \dots + x_ic_{p,i} \tag{10}$$

serial number	Leak aperture size (mm)	Hydrogen-doped ratio (%)	Wind speed (m/s)	Distance between air inlet and outlet (m)
1	10	20	2.4	200
2(Standard operating conditions)	20	20	2.4	200
3	30	20	2.4	200
4	40	20	2.4	200
5	20	0	2.4	200
6	20	5	2.4	200
7	20	10	2.4	200
8	20	15	2.4	200
9	20	20	1.4	200
10	20	20	1.9	200
11	20	20	2.9	200
12	20	20	2.4	50
13	20	20	2.4	100
14	20	20	2.4	150

Table 2. Parameters of operating conditions.

$$c_{v,m} = x_1 c_{v,1} + x_2 c_{v,2} + x_3 c_{v,3} + \dots + x_i c_{v,i} \quad (11)$$

$$k_m = \frac{c_{p,m}}{c_{v,m}} \quad (12)$$

Where, x_i is the percentage of the i gas; m is the average molar mass, kg/mol; $c_{p,m}$ is the specific heat capacity at constant pressure, J/(kg•K); $c_{v,m}$ is the constant volume specific heat capacity, J/(kg•K).

Leakage flow rate The temperature of the manhole space, leaking point, intake, and exhaust is set to 300 K, and the pressure is set to standard atmospheric pressure during the first stage of hydrogen-containing natural gas leakage. One way to think about the gas leaking process is as a small hole leakage problem³⁴.

According to the critical pressure ratio classification, the natural gas flow velocity can be divided into supersonic and subsonic. The critical pressure ratio is:

$$\beta = \left(\frac{2}{k+1} \right)^{\frac{k}{k-1}} \quad (13)$$

Where, k is the isentropic index of gas.

When $P_a/P_2 > \beta$, the gas flow rate of the leakage hole is subsonic, and the leakage rate is:

$$Q = C_0 P_2 A \sqrt{\frac{M}{ZRT_2} \frac{2k}{k-1} \left[\left(\frac{P_a}{P_2} \right)^{\frac{2}{k}} - \left(\frac{P_a}{P_2} \right)^{\frac{k-1}{k}} \right]} \quad (14)$$

Where, P_a is atmospheric pressure, Pa; P_2 is the pipeline pressure, Pa; C_0 is the correction coefficient of orifice leakage, and the circular orifice is taken as 1; A is the area of leakage orifice, m²; M is the molar mass of the leaking gas, kg/mol.

When $P_a/P_2 \leq \beta$, the gas flow rate of the leakage hole is sonic, and the leakage rate is:

$$Q = C_0 P_2 A \sqrt{\frac{M}{ZRT_2} \left(\frac{2}{k+1} \right)^{\frac{k+1}{k-1}}} \quad (15)$$

Wind speed The normal ventilation frequency must be at least six times per hour, and the accident ventilation frequency must be at least twelve times per hour, as per the Chinese national standard GB 50,838–2015, “Technical Specifications for Urban Integrated pipe Corridor Engineering.” The average wind velocity method³⁵ was used to determine the ventilation velocity of air intake under mechanical ventilation settings.

$$v = \frac{nV}{3600A_0} \quad (16)$$

where, v is the average wind speed of the inlet, m/s; n is the ventilation frequency, times/h; V is the volume of the pipe gallery, m³; A_0 is the area of the inlet, m².

Equation (17) can be used to determine the wind speed corresponding to various ventilation frequencies in a two-dimensional simplified numerical model with model width as unit length. Table 3 displays the results of the computation.

n (times/h)	6	8	10	12
v (m/s)	1.4	1.9	2.4	2.9

Table 3. Calculation results of wind speed at different ventilation frequencies.

Hydrogen-doped ratio (%)	0	5	10	15	20
Upper explosion limit (%)	15	15.62	16.31	17.05	17.86
Lower explosion limit (%)	5	4.93	4.87	4.81	4.76

Table 4. Upper and lower explosion limits of mixed gases.

Object	Boundary type	Remark
Point of leakage	Quality Inlet	Mass flow of hydrogen-doped natural gas
Air inlet	Speed Inlet	Wind speed
Air outlet	Pressure Outlet	Standard atmosphere
Left and right channel	Pressure Outlet	Standard atmosphere
Pipeline	Wall	-
Top, bottom and side of pipe gallery	Wall	-
Cabin	Fluid domain	Initially air

Table 5. Boundary condition settings.

Upper and lower limits of explosion The explosion limit of hydrogen-doped natural gas is calculated using Le Chatelier's mixing rule. The explosion limit of methane is 5.00%~15.00%, and the explosion limit of hydrogen is 4.00%~75.60%. Le Chatelier's law is as Eq. (17), (18).

$$LEL_{\text{mix}} = 1 / \left(\frac{y_1}{LEL_1} + \frac{y_2}{LEL_2} + \frac{y_3}{LEL_3} + \dots + \frac{y_i}{LEL_i} \right) \quad (17)$$

$$UEL_{\text{mix}} = 1 / \left(\frac{y_1}{UEL_1} + \frac{y_2}{UEL_2} + \frac{y_3}{UEL_3} + \dots + \frac{y_i}{UEL_i} \right) \quad (18)$$

Where, LEL_{mix} and UEL_{mix} are the upper and lower limits of the explosion of the mixed gas, y_i is the volume fraction of a kind of gas in the mixed gas; s is the total number of gas species contained in the mixed gas; LEL_i and UEL_i are the upper and lower explosion limits of a certain kind of gas in a mixed gas.

The parameters of mixed gas under different hydrogen mixing ratios can be obtained by calculation, as shown in Table 4.

Boundary conditions and solution setup

The FLUENT finite volume method was used to solve the equations related to the conservation of mass, momentum, and energy³⁶. A hydrogen-doped natural gas leakage port, an air inlet, an air outlet, two side outlets, a pipe wall, and a pipe corridor wall comprise the model's primary boundaries. The combination of CH_4 and H_2 is separated into various proportions within the group, and the temperature is set at 300 K. The mass flow rate inlet is chosen as the boundary condition of the hydrogen-doped natural gas leakage port^{10,36}. The group is separated into air, and the air inlet is configured as the speed inlet. The Outlet boundary condition often refers to the gas outlet end, which is set as a Pressure Outlet to simulate the gas diffusion perpendicular to the wall under the action of the airflow. In the setting of the wall boundary, since thermal analysis is not the focus of this paper, the research wall is set as an isothermal wall with a temperature of 300K^{17,36}. The boundary condition Settings are shown in Table 5. It is assumed that the flow field in the calculation area is in a stable state before the leakage of the natural gas pipeline, and the velocity and concentration of methane and hydrogen are 0³⁶.

Grid-independent verification

The area with a high gradient of data change, particularly the area surrounding the leak hole, needs to be locally adjusted in order to lower computing complexity and increase numerical accuracy. Wind speed of 2.4 m/s, intake and outlet spacing of 200 m, HBR of 20%, and leakage size of 20 mm were the parameters used to study grid independence. Four grid schemes with grid numbers of 1,202,370, 1,523,970, 2,172,970 and 3,430,000 were used for calculation. The variation of methane concentration in the vertical Y direction of the leak hole location under the four grid schemes is shown in Fig. 3(a). Mesh quality verification is usually evaluated through a series of quantitative metrics, such as maximum skew, aspect ratio, etc³⁷. Therefore, the maximum skew of the four meshes is compared, and the results are shown in Fig. 3(b). As can be seen from the figure, when the number of

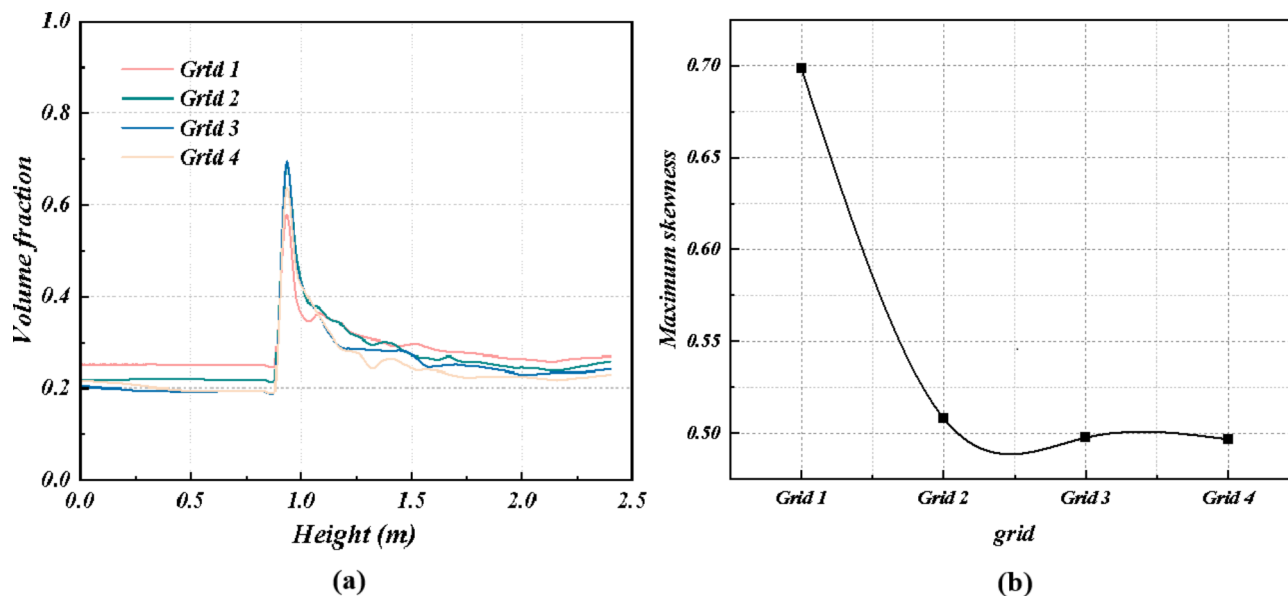


Fig. 3. Grid validation data (a) Simulation results verify (b) Comparison of maximum skewness.

grids reaches 3,430,000, the calculation results gradually tend to be stable. In order to meet the requirements of simulation accuracy and efficiency, the number of meshes used in subsequent simulations was 3,430,000.

Verification of accuracy

A leakage and diffusion experiment of hydrogen-doped natural gas in a home kitchen was chosen for comparative analysis in order to confirm the accuracy of the numerical model⁸. The kitchen model data was obtained from the literature and had dimensions of 2.5 m by 1.6 m by 2.6 m, as illustrated in Fig. 4(a). The leak hole is 8 mm in size, with a leakage flow rate of 4 and 8 Nm³/h, 80% nitrogen, and 20% helium. The monitoring points 1 (0.76, 0.50, 1.15), 5 (1.50, 0.50, 1.68), 8 (1.50, 0.50, 0.20), and 9 (0.50, 1.55, 2.05) are displayed in Fig. 4(b) and (c). Simulations and experimental findings on oxygen concentration. At these two instances, it is evident that the trend of the computer findings and the experimental results is consistent. These two leakage flows had maximum and average absolute deviations of 1.20% and 1.20%, respectively, 34% and 1.60% and 2.19%. The numerical model's dependability is confirmed by the deviation value, which is within an acceptable range and quite tiny.

Analysis of single influencing factors on the diffusion behavior of hydrogen-doped natural gas

Given that the city comprehensive pipe gallery's gas tank has a medium- and low-pressure hydrogen-doped natural gas pipeline leak, this part includes varying wind speeds (1.4, 1.9, 2.4, and 2.9 m/s), input and outlet spacing (50, 100, 150, and 100 m), hydrogen mixing ratio (0, 5%, 10%, 15%, 20%) and leakage port size (10 mm, 20 mm, 30 mm, 40 mm) Influence on leakage and diffusion characteristics of hydrogen-doped natural gas in gas tanks in urban integrated pipeline corridors.

Leakage aperture size

Figure 5 shows the distribution of the leakage gas concentration field and velocity field in the pipe gallery under different leakage port sizes (when the air inlet and outlet spacing is 200 m, HBR is 20%, and the wind speed is 2.4 m/s).

As shown in Fig. 5(a), as the size of the leakage increases, the high-volume fraction of gas above the pipe gallery becomes more concentrated, while hydrogen-doped natural gas accumulates more around the leakage port beneath the pipeline. The concentration beneath the air inlet is mainly concentrated at the top of the pipe gallery, though it remains lower than that at the air outlet. Notably, when the leakage port is 10 mm, a stratification phenomenon of hydrogen-doped natural gas appears in the pipe gallery. This layering effect gradually diminishes as the leakage port size increases. When the leakage is 40 mm, the overall concentration level in the pipe gallery is significantly high, resulting in an extremely hazardous situation.

As seen in Fig. 5(b), the increase in leakage size alters the streamline structure within the pipeline gallery, with a substantial expansion of the high-velocity diffusion area. When the leakage port size increases to 20 mm, the length of the vortex area beneath the air inlet increases, causing the streamlines downstream of the pipe gallery to no longer converge, and the concentration distribution becomes broader. As the leakage port size reaches 40 mm, the vortex structure beneath the air inlet disappears. The gas accumulation above the pipe gallery increases, and the leakage velocity above the leakage port rises sharply. Simultaneously, part of the leaking gas is carried into the middle and lower spaces of the pipe gallery, leading to an increase in gas concentration in the lower areas.

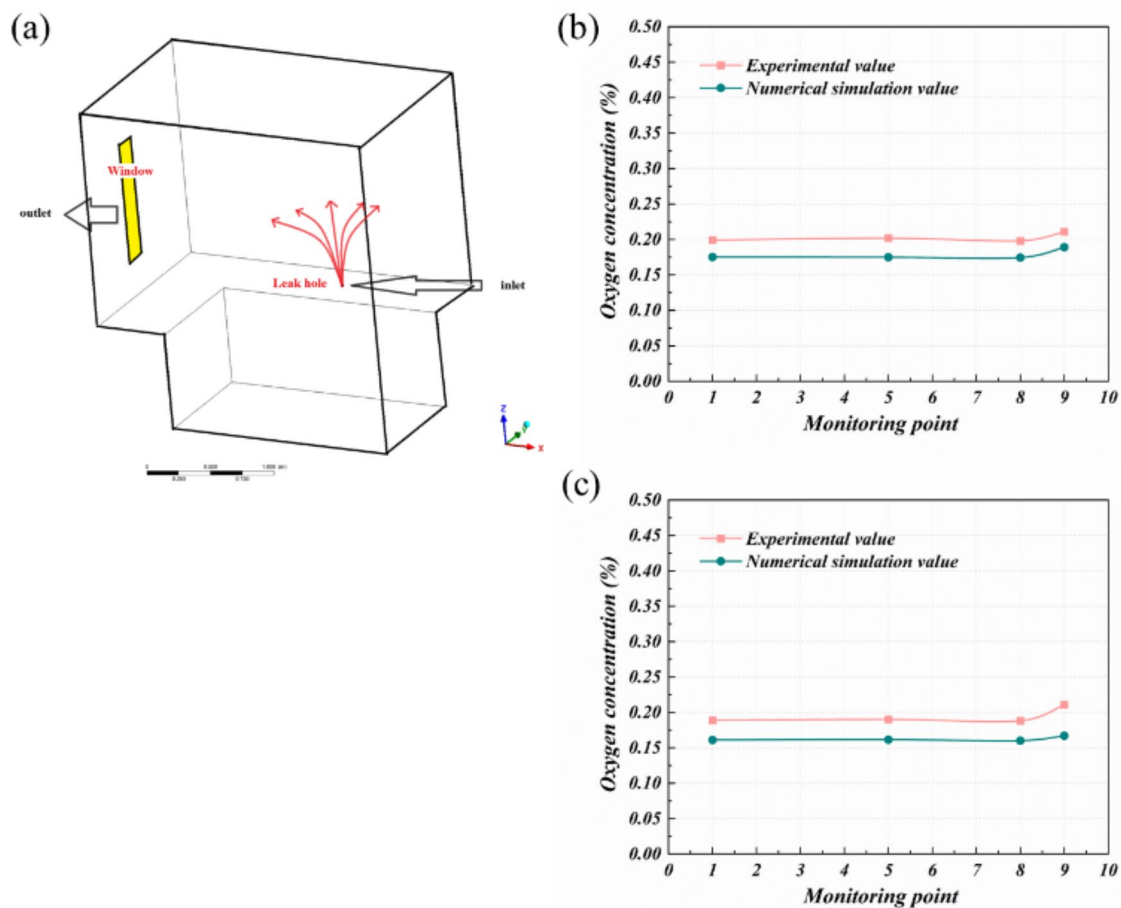


Fig. 4. Accuracy verification (a) 3D model of the kitchen (b) Comparison of simulation results and experimental results when the leakage flow rate is 4Nm³/h (c) Comparison of the simulation results and experimental results when the leakage flow rate is 8Nm³/h.

Figure 6 illustrates the variation of the explosion volume of hydrogen-doped natural gas at different leak orifice sizes. Compared with the standard operating condition, when the leakage aperture size increased from 20 mm to 40 mm, the explosion volume of CH₄ decreased by 52.99% and 99.88% respectively. The explosion volume of H₂ increased by 143.48% and 214.58%. When the leakage aperture size is reduced from 20 mm to 10 mm, the explosion volume of CH₄ is reduced by 29.23% respectively. The H₂ explosion volume is reduced by 100%. Among them, the larger the leakage hole, the smaller the methane explosion volume in the pipe gallery. This phenomenon is mainly because when the natural gas leakage is large, the concentration of methane in the confined space will increase rapidly, and the methane concentration will soon exceed the upper limit of the explosion (UEL). After exceeding the UEL, the concentration of methane in the gas mixture is too high, and the oxygen is insufficient to support combustion or explosion. As a result, this part of the area where the concentration exceeds the UEL is no longer explosive but “out” of the blast range. The explosion volume of hydrogen can be increased all the time because the upper and lower explosion limits of hydrogen are wide and less limited by the upper and lower explosion limits. As the leakage increases, the concentration of hydrogen rises rapidly in the confined space, and the upper limit of the explosion is less exceeded, resulting in an increase in the effective explosion volume.

Hydrogen-doped ratio

Figure 7 shows the distribution of the leakage gas concentration field and velocity field in the pipe gallery under different hydrogen doping ratios (when the spacing between the air inlet and outlet is 200 m, the leakage aperture size is 20 mm, and the wind speed is 2.4 m/s).

Figure 7(a) shows the distribution of the leakage gas concentration field in the pipe gallery. Compared with natural gas, when the hydrogen blending ratio is 5% and 10%, the concentration field does not change obviously,

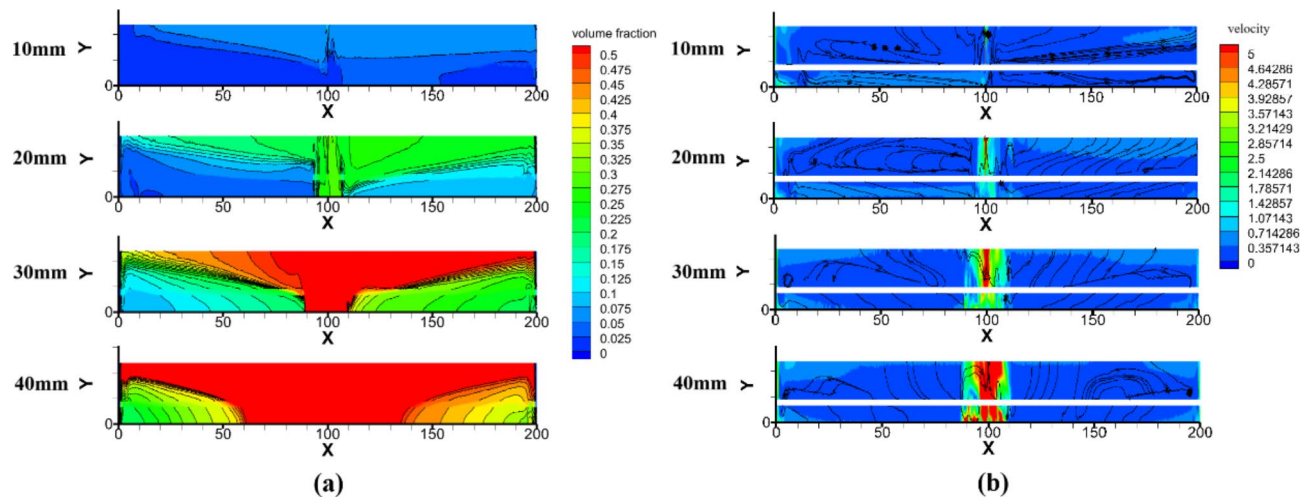


Fig. 5. Distribution of hydrogen-doped natural gas under different leakage pore sizes (a), concentration field (b), velocity field.

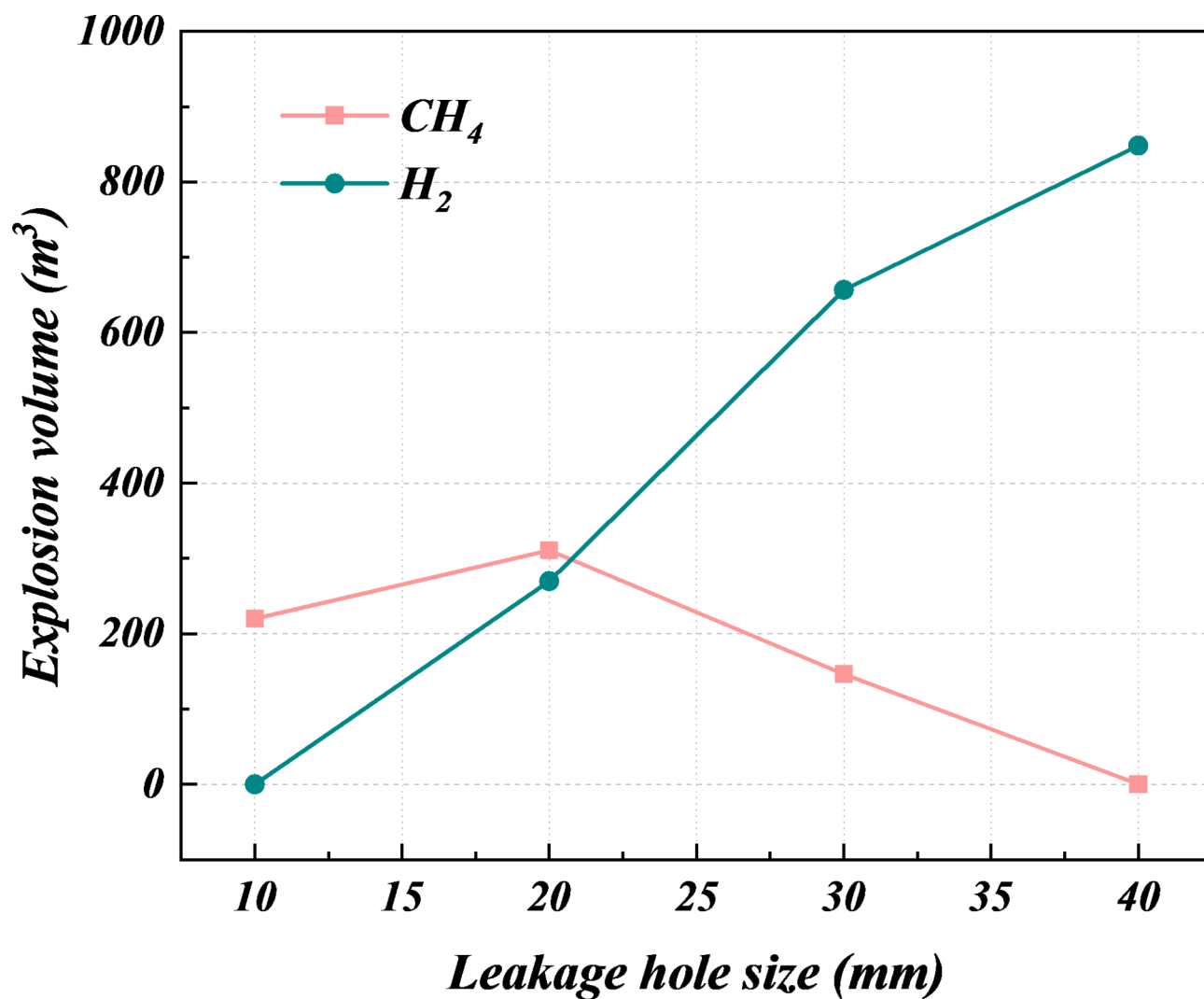


Fig. 6. Changes in the explosion volume of hydrogen-doped natural gas under different leakage orifice sizes.

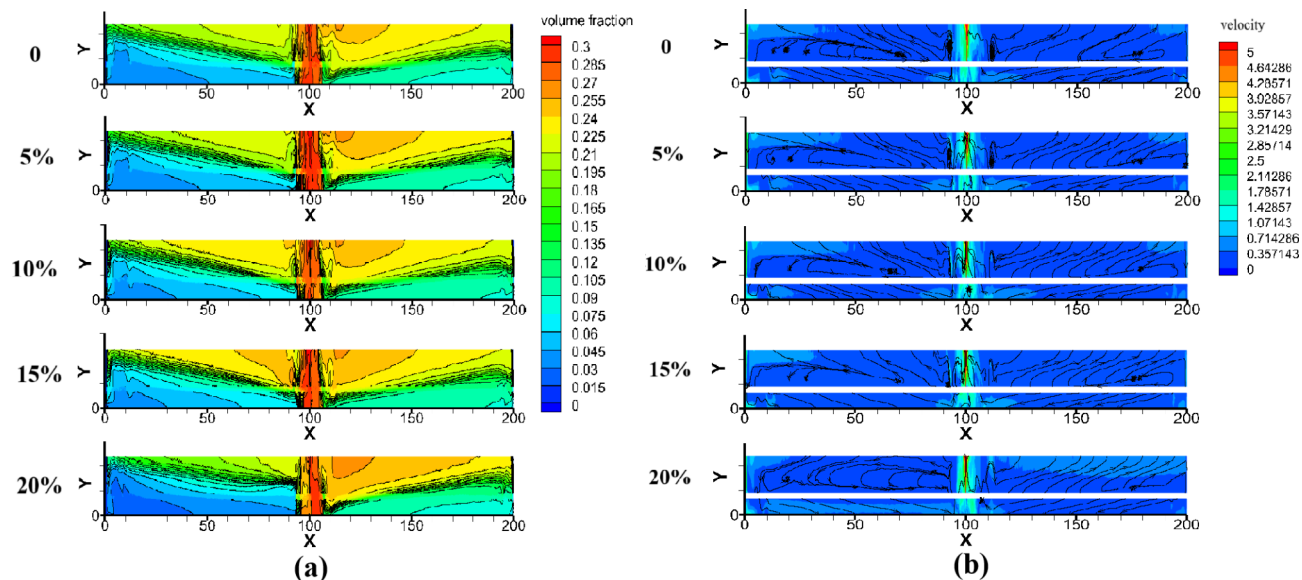


Fig. 7. Distribution of hydrogen-blended natural gas with different hydrogen doping volume ratios (a), concentration field (b), velocity field.

and the concentration distribution law is similar. When the hydrogen doping ratio is increased to 15%, the high volume fraction of gas near the air inlet of the leakage port gathers above the pipe gallery, and the gas concentration distribution near the air outlet has little effect. When the HBR value is 20%, the downwind danger area near the outlet increases significantly, but the gas concentration above the pipe gallery in the direction of the air inlet is low, and most of the hydrogen-doped natural gas gathers below the air outlet and at the top of the pipe gallery. It is shown that hydrogen mixing will increase the safety risk of public pipe corridors after pipeline leakage. Figure 7(b) shows the velocity field distribution of leakage gas in the pipe gallery. Observing the velocity streamlines diagram of different hydrogen doping ratios, it can be found that hydrogen doping does not significantly change the streamline structure of the pipeline corridor but only lifts the vortex line near the air inlet and increases the length of the vortex area so that a fast flow area is formed under the pipeline on the left side of the leakage port so that the gas is not easy to accumulate at the bottom of the pipe corridor.

As can be seen from Fig. 8, Compared with the standard condition, the explosion volume of CH_4 is reduced by 9.78%, 10.78%, 13.55% and 12.25% respectively when the hydrogen mixture ratio is reduced from 20% to 0. The explosion volume of H_2 is reduced by 86.55%, 100%, 100%, 100%. In particular, when the hydrogen mixture ratio is 0–10%, the explosion volume of H_2 is close to 0. the larger the hydrogen doping ratio, the larger the explosion volume of methane and hydrogen in the pipe gallery, which is mainly related to the explosion limit characteristics and their behavior in the gas mixture. One is that the explosion limit (LEL and UEL) of hydrogen is wider than that of methane. With the increase in the number of hydrogen gas integrals in the leaked gas, the range of hydrogen concentrations that can form explosive mixtures in the pipe gallery increases. The second is that hydrogen diffuses faster than methane. After being mixed with hydrogen, the mixed gas diffuses faster in the pipe gallery and is easy to form a homogeneous mixture in a larger area. This rapid diffusion property may allow larger volumes of gas mixtures to reach the explosive concentration range, resulting in an increase in the explosive volumes of methane and hydrogen. Therefore, in relatively enclosed spaces such as pipe corridors, the explosion volume of methane and hydrogen increases significantly. This phenomenon requires special attention in industrial safety management to prevent a greater risk of explosion due to increased hydrogen doping.

Wind speed

Figure 9 shows the distribution of the leakage gas concentration field and velocity field in the pipe gallery at wind speed (when the spacing between the air inlet and outlet is 200 m, the HBR is 20%, and the leakage aperture size is 20 mm).

Figure 9(a) shows the distribution of the leakage gas concentration field in the pipe gallery. It can be seen that with the increase in wind speed, the gas concentration at the air inlet decreases significantly, and the hydrogen-doped natural gas with a high volume fraction no longer gathers above the pipe gallery at the air inlet. According to the concentration distribution of hydrogen-doped natural gas at the air outlet, it can be seen that with the increase in wind speed, the high volume fraction of gas accumulation above the pipe gallery at the air outlet and the accumulation degree of hydrogen-doped natural gas below the pipeline is also reduced. On the whole, the increase in wind speed reduces the concentration of hydrogen-doped natural gas in the pipe gallery as a whole, and the danger range is reduced. Figure 9(b) shows the velocity field distribution of leaked gas in the pipe gallery. With the increase of wind speed, the vortex area below the air inlet gradually increases, and more hydrogen-doped natural gas with a high volume fraction enters the downstream of the pipe gallery through the vortex, which accelerates the gas flow in the overall pipe gallery space. The velocity streamlines below the

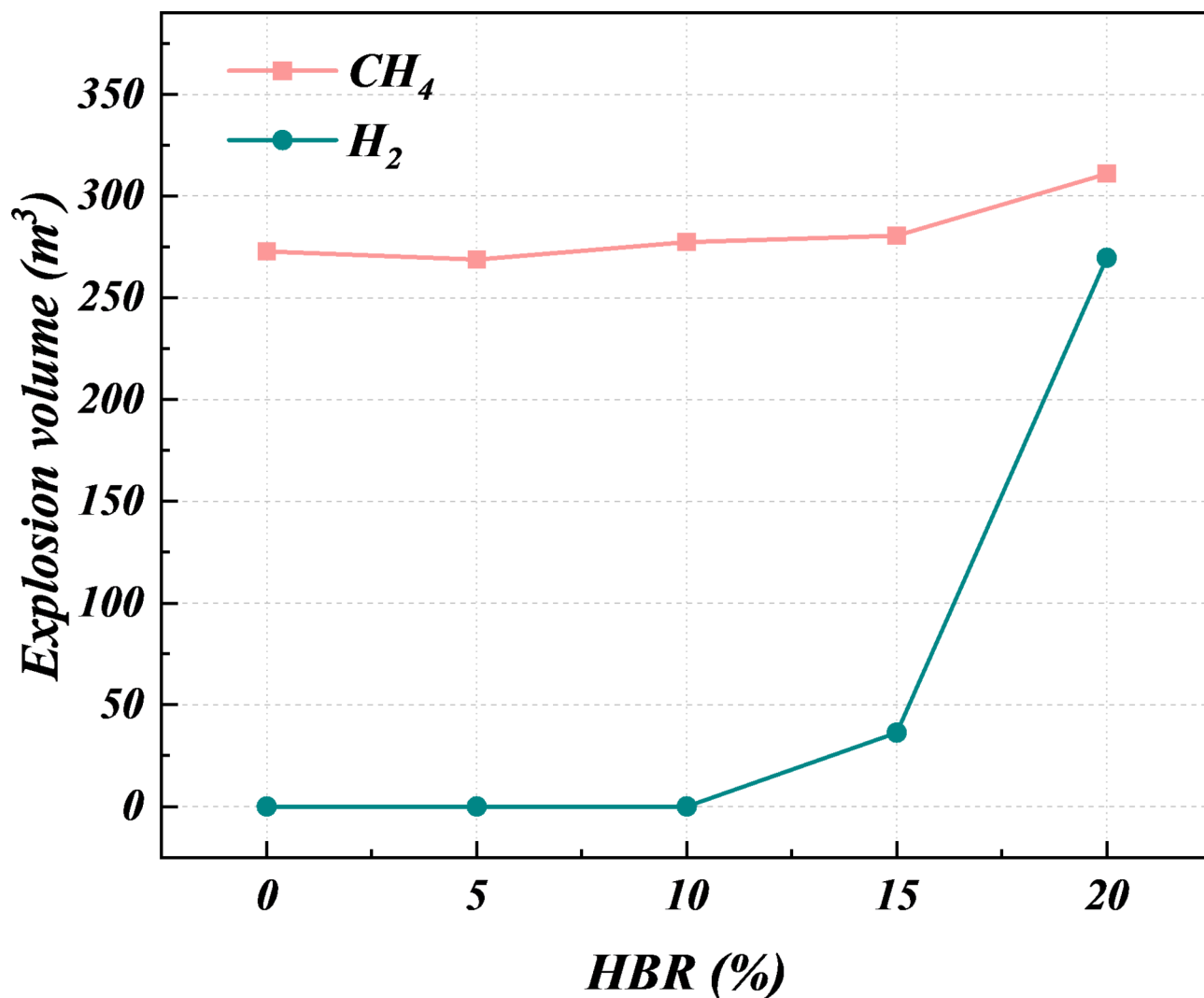


Fig. 8. Variation of the explosion volume of hydrogen-doped natural gas under different hydrogen-doped volume ratios.

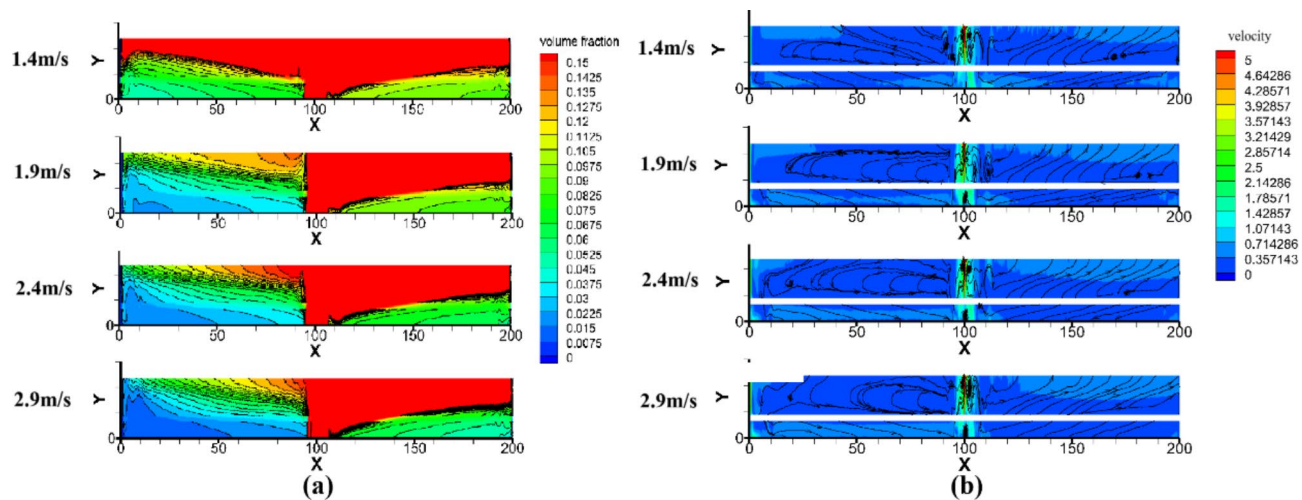


Fig. 9. Distribution of hydrogen-doped natural gas at different wind speeds (a) concentration field (b) velocity field.

air outlet gradually move downward, pushing the high volume fraction of gas under the pipe to flow to the air outlet, which reduces the accumulation of hydrogen-doped natural gas at the bottom of the pipe gallery to a certain extent.

As can be seen from Fig. 10, Compared with the standard condition, when the inlet wind speed increases from 2.4 m/s to 2.9 m/s, the explosion volume of CH_4 decreases by 35.68% and that of H_2 decreases by 20.50%. When the inlet wind speed decreased from 2.4 m/s to 1.4 m/s, the explosion volume of CH_4 first decreased by 3.79% and then increased by 20.43%. The explosion volume of H_2 first decreases by 0.28% and then increases by 8.91%. So the methane explosion volume dropped even more. In confined spaces, the larger the ventilation velocity, the smaller the explosion volume of methane and hydrogen leakage, which is mainly related to the dilution effect of ventilation on methane and hydrogen concentrations and the control of mixed gas concentrations. Ventilation can dilute the concentration of leaking gases. As the number of ventilations increases, fresh air entering the space can dilute leaked methane and hydrogen, making them less concentrated in the air. When ventilation is strong enough, the concentration of methane and hydrogen falls below the lower explosion limit (LEL), reducing or completely eliminating the volume of explosive gases. It can be seen that with proper ventilation design, the leaking hydrogen-doped natural gas can be quickly controlled below the safe concentration, thus effectively preventing the risk of explosion.

The effect of ventilation on the volume reduction of methane and hydrogen explosions in confined spaces varies, mainly related to the explosion limit, molecular mass, and diffusivity of methane and hydrogen. Methane and hydrogen have different explosion limits. Methane has a narrow explosion limit of 5–15% (volume fraction), while hydrogen has a wide explosion limit of 4–75%. This means that even at low concentrations, hydrogen can still cause an explosion, while methane only explodes in a relatively small concentration range. Secondly, hydrogen has a smaller molecular mass (2 g/mol) and, therefore, diffuses faster in the air; Hydrogen diffuses more easily and occupies a larger space. In summary, although ventilation can reduce the explosion volume of methane and hydrogen, due to the wide explosion limit, fast diffusion, and fast flame propagation speed of

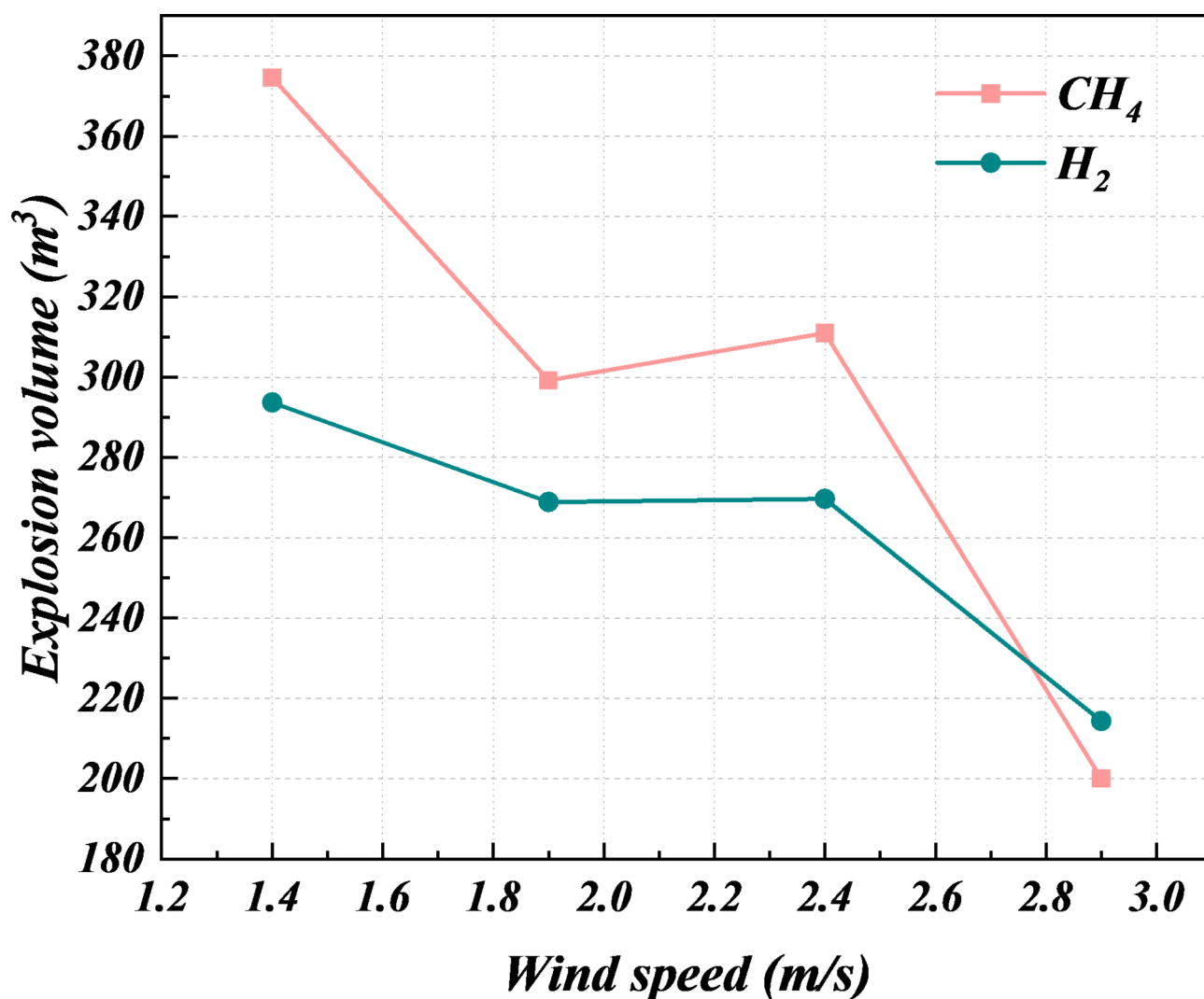


Fig. 10. Variation of the explosion volume of hydrogen-doped natural gas at different inlet wind speeds.

hydrogen, ventilation often requires stricter control and more effective ventilation design to reduce the risk of hydrogen explosion.

Distance between air inlet and outlet

Figure 11 shows the distribution of the leakage gas concentration field and velocity field in the pipe gallery under different inlet and outlet spacing (when the leakage aperture size is 20 mm, the HBR is 20%, and the wind speed is 2.4 m/s).

Figure 11(a) shows the distribution of the leakage gas concentration field in the pipe gallery. On the whole, when the spacing between the air inlets and outlets is 50 m, the overall concentration level of the pipe gallery is the lowest, and the area of high-volume hydrogen-doped natural gas distribution is the smallest. When the spacing is 50 m, the second air inlet is located above the leakage, resulting in a low distribution of hydrogen-doped natural gas upstream of the pipe gallery, and at the same time, it works together with the air inlet at 200 m to aggregate the gas at the air outlet of 150 m, resulting in the smallest aggregation of hydrogen-doped natural gas with high volume fraction. When the spacing is 100 m, the air outlet is located above the leakage port, and the leaked gas can directly escape out of the pipe gallery due to the joint action of its own jet and the air inlet on both sides, but because there is only one air outlet, the overall concentration level is higher than that of 50 m. As the spacing between the air inlets and outlets increases, the overall concentration level increases, and the hazard range increases. It shows that the distance between the air outlet and the leakage point greatly affects the concentration level of hydrogen-doped natural gas in the pipe gallery.

Figure 11(b) shows the velocity field distribution of leakage gas in the pipe gallery. Observing the cloud image, it can be seen that the increase of the spacing between the inlet and outlet has little effect on the velocity on the center line of the jet but completely changes the streamline of the diffusion of hydrogen-doped natural gas. When the spacing between the air inlets and outlets is 50 m, the air intakes on both sides and in the center of the pipe gallery promote the diffusion of hydrogen-doped natural gas to the air outlets on the left and right sides of the leakage port, and the overall fluidity is strong. When the spacing between the air inlet and outlet is 100 m, the air outlet is located above the leakage port, and the air inlets on both sides promote the diffusion of hydrogen-doped natural gas out of the pipe gallery. The concentration distribution of the air inlet and outlet spacing of 150 m and the spacing of 200 m is similar, but the shorter the spacing, the shorter the distance of hydrogen-doped natural gas diffusion, which is conducive to the reduction of the concentration level of hydrogen-doped natural gas in the pipe gallery.

As shown in Fig. 12, Compared with the standard working condition, when the inlet and outlet spacing is reduced from 200 m to 50 m, the explosion volume of CH_4 is reduced by 49.81%, 3.21% and 99.92%, and the explosion volume of H_2 is reduced by 8.12% and 100%. This phenomenon is closely related to factors such as ventilation efficiency, gas diffusion behavior, and concentration distribution. When the spacing between the air inlets and outlets of the pipe gallery is large, the ventilation efficiency will be reduced. As the airflow passes through the corridor over long distances, it gradually weakens, resulting in a decrease in the velocity of the airflow. The reduced ventilation efficiency means that the leaking gas cannot be quickly discharged or diluted in the pipe gallery and tends to accumulate in some areas, and methane and hydrogen can easily accumulate and reach concentrations between the lower explosion limit (LEL) and the upper limit (UEL), thus increasing the explosion volume in that area. The long-distance air inlet and outlet will lead to the formation of a clear gas concentration gradient in the pipe gallery; that is, the concentration is higher in the area near the leakage source, and the concentration may be lower in the area away from the air outlet.

Among them, when the spacing between air inlets and outlets increases from 100 m to 200 m, the explosion volume of methane decreases first and then increases. This is because the explosive volume of hydrogen gas

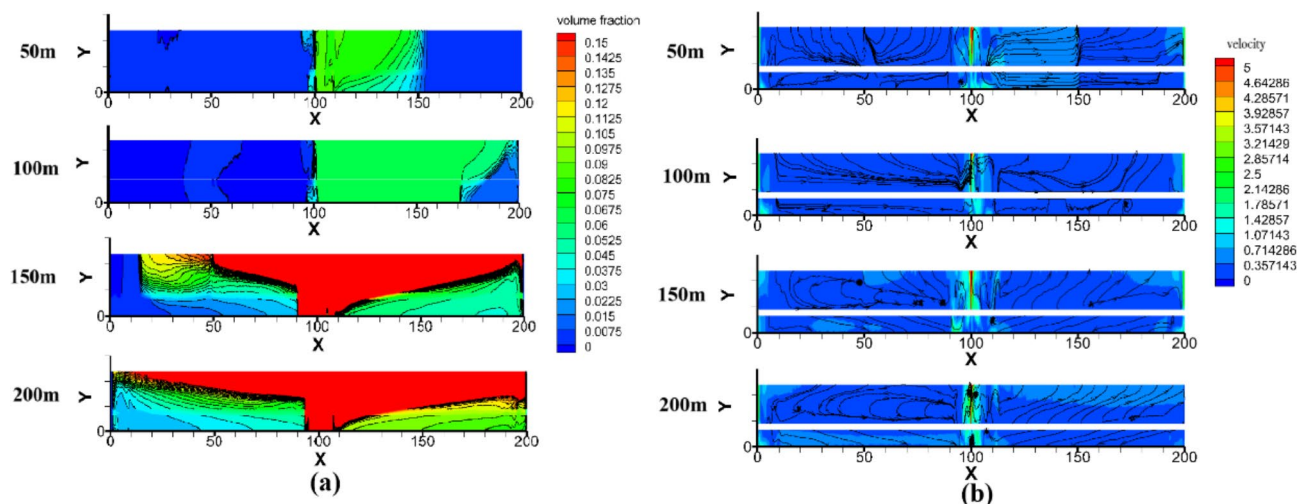


Fig. 11. Distribution of hydrogen-doped natural gas at different inlet and outlet spacing (a) concentration field (b) velocity field.

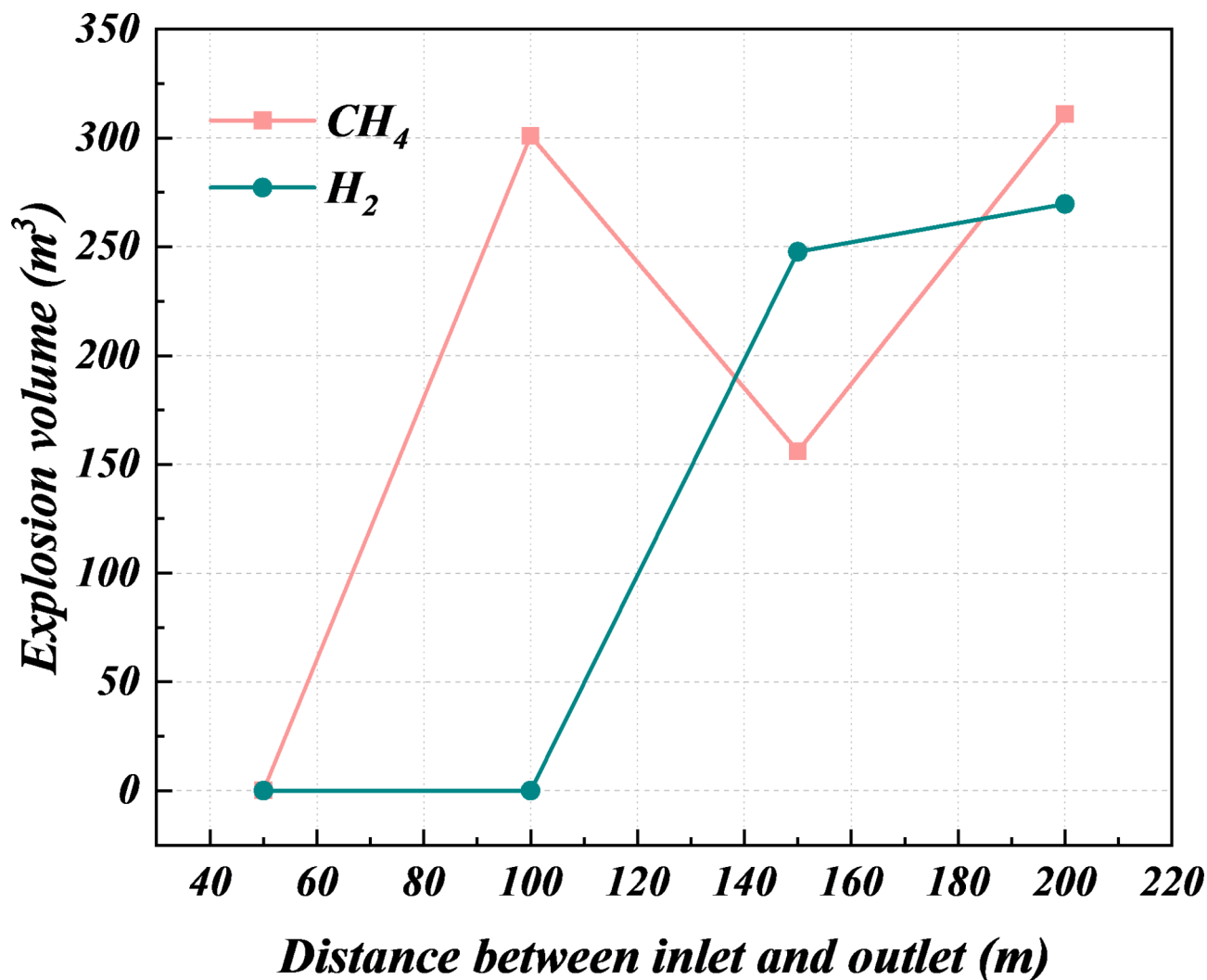


Fig. 12. Variation of the explosion volume of hydrogen-doped natural gas at different inlet and outlet spacing.

increases rapidly due to the accumulation of airflow, which occupies a large amount of pipe gallery space. Then, with the increase of the spacing between the air inlets and outlets, the accumulation effect of the airflow is further strengthened, the volume fraction of hydrogen is smaller, and the diffusion degree is limited, so the explosion volume of methane increases.

Intelligent prediction model of explosive gas volume in pipe corridor based on GA-BPANN

Data processing

Latin hypercube sampling

Latin Hypercube Sampling (LHS) is a hierarchical stochastic process that provides an efficient way to sample variables from a given distribution³⁸. For the four factors studied, LHS was sampled within their respective ranges. The value ranges are leakage flow velocity (0.0247–0.3958 kg/s), hydrogen doping ratio (0–20%), wind speed (1.4–2.9 m/s), and air inlet and outlet spacing (50–200 m). The sampled experimental data are shown in Table 6.

Data normalization

In order to eliminate the influence of dimensions on the prediction results, the data need to be normalized³⁹. The maximum-minimum normalization method is usually used to normalize the sample data into the [0,1] interval, as shown in Eq. (19).

$$x'_i = \frac{x_i - x_{\min}}{x_{\max} - x_{\min}} \quad (19)$$

Leakage flow rate (kg/s)	Hydrogen-doped ratio (%)	Wind speed (m/s)	Distance between inlet and outlet (m)	Methane explosion volume (m ³)	Hydrogen explosion volume (m ³)
0.2872	2.8043	2.8575	71.8593	71.0014	0.0000
0.0889	19.9732	1.6504	138.1450	289.9227	116.3987
0.3068	6.4242	1.7853	183.9701	117.0000	66.8000
0.0676	8.7927	2.0205	113.1919	466.5185	0.0000
0.0793	18.5265	1.4710	148.6257	426.6556	0.0017
0.2577	12.4865	2.4546	65.8082	67.3860	0.0180
0.1554	17.7863	2.1012	198.0606	288.0000	453.0000
0.2760	10.8459	2.8403	119.5005	41.6289	118.0554
0.3362	8.8404	2.0533	144.8052	131.2860	334.6379
0.2368	0.5496	2.3694	53.7505	502.3306	0.0000
0.3276	15.9449	1.6063	167.4943	133.0000	465.0000
0.1233	11.9129	2.0083	154.0326	7.7400	0.7200
0.3188	12.3271	1.6222	63.3432	131.6763	202.9453
0.3896	14.3833	2.6070	116.0626	59.0256	257.8307
0.3755	1.1572	2.7468	90.3521	22.3216	0.0000
0.0279	9.7534	1.9516	124.0087	135.3084	0.0000
0.1644	18.0241	2.5005	96.1416	529.5296	0.0021
0.1735	16.2582	1.8193	99.9181	0.0016	0.0000
0.2974	3.4357	2.2819	74.7305	58.9960	0.0000
0.2405	4.0063	2.7091	81.7583	45.2175	0.0000
0.3719	1.6218	2.3585	51.5230	69.7739	0.0000
0.1704	0.1293	1.9244	188.9158	188.0000	0.0000
0.1131	11.2047	1.8691	134.0818	180.4032	0.0000
0.0348	15.2933	2.2035	193.0167	189.0000	0.0001
0.3499	17.4653	2.1256	68.4866	48.1894	255.9273
0.1060	12.9350	1.9614	185.7828	247.0000	24.9000
0.1826	2.7023	2.3299	164.1375	285.0000	0.0000
0.2300	15.0818	2.5619	127.9042	87.9882	278.6884
0.1163	3.7279	2.1439	105.9294	0.0244	0.0000
0.2668	4.5889	2.1666	84.0120	29.4248	0.0000
0.2130	2.2354	1.5750	157.1555	179.0000	0.0000
0.0988	4.9589	1.4636	79.3089	298.3498	0.0000
0.3519	5.6998	1.8046	59.8666	50.8564	0.0000
0.0485	6.9666	1.8947	159.1263	590.0000	0.0000
0.1454	10.5793	2.4045	141.2282	176.0432	0.0040
0.1300	10.1666	2.7963	150.0187	156.0000	0.0001
0.2223	7.7953	2.7755	133.8573	107.4117	97.0210
0.0424	8.3670	2.2435	102.9536	453.8327	0.0000
0.1912	18.9122	1.7455	93.6460	167.8178	553.5444
0.0579	16.4015	2.6768	175.2773	425.0000	0.0001
0.0746	13.4582	2.6352	86.8549	228.0961	0.0001
0.3643	6.0115	2.5220	170.4315	41.7000	160.0000
0.1401	7.4614	2.5633	163.1555	109.0000	0.0000
0.2531	1.2454	1.5318	176.8068	223.0000	0.0000
0.3824	19.4181	2.4340	112.5867	87.3689	357.3238
0.1955	17.0346	2.2494	128.4898	116.4876	245.0322
0.3065	13.9129	1.7240	196.5842	286.0000	0.0000
0.3399	9.5497	1.5152	108.2354	63.5360	74.2862
0.2096	5.4764	2.6805	57.9015	106.9156	0.0000
0.2785	14.5096	1.6728	179.5797	201.0000	434.0000

Table 6. Experimental data.

Where, x_i and x'_i is the data before and after standardization, x_{\max} and x_{\min} is the maximum and minimum value of the sample data.

GA-BP neural network creation

The way the human brain functions is the basis for modeling backpropagation neural networks. The most popular neural network model at the moment is the BPNN algorithm. An input layer, a hidden layer, and an output layer are all part of BPNN⁴⁰. The acquired simulation data is used to train and learn hidden layer neurons, which reflect the input-output relationship. Following adequate education, the study's findings were reviewed. The trained model can be used to forecast new outputs once the learning outcomes are approved. Thus, BPNNs can be used to address complicated nonlinear problems. The explosion danger volume of hydrogen and methane in the pipe gallery was predicted in this investigation using BPNN.

In this study, the leakage orifice (d), hydrogen doping ratio (HBR), wind speed (v), and inlet and outlet spacing (D) were found in the input layer. There are four input points in the input layer, and the output layer includes the explosion volume (V_{gas}) of methane and hydrogen. The relationship between input and output can be expressed as Eq. (20):

$$V_{\text{gas}} = f(d, D, v, HBR) \quad (20)$$

A BPNN with a three-layer prediction model was developed in order to derive the explosion volume (V) of hydrogen and methane at the maximum horizontal diffusion distance from this unknown function. As seen in Fig. 14⁴¹, there are one node in the output layer and four nodes in the input layer. The number of neurons in the hidden layer can be obtained according to the Kolmogorov theorem or through the training test of different hidden layer node numbers. The more nodes, the easier to overfit, the fewer nodes, will increase the error. Usually, the approximate interval of N is determined by the equations (21) and (22), and then the optimal number N is obtained by many experiments⁴².

$$N = \sqrt{(m+n)} + c \quad (21)$$

$$\frac{(m+n)}{2} \leq h \leq (m+n) + 10 \quad (22)$$

where, N is the number of hidden layer nodes, m is the number of output layer nodes, n is the number of input layer nodes, and c is a constant of [0,10].

The training effect is optimum when N is 4, according to a comparison and analysis of the prediction outcomes under the number of nodes in various hidden layers. As a result, Fig. 13 displays the topology of BPNN, which is 4-4-1. The learning rate is set to 0.01; the minimum training error is 1×10^{-6} ; the training times are 1000 times; the maximum number of failures is 6 times; the output layer neuron's transfer function is chosen as a pure line; and the hidden layer neuron's transfer function is chosen as transit.

Genetic algorithm optimization of neural networks

The accuracy of the final prediction findings is significantly impacted by the weights and thresholds that are first established in BP-ANN. Local optimality may arise during model execution if these parameters are assigned at random using conventional procedures^{43,44}. The genetic algorithm to optimize the back propagation neural network can improve the generalization ability of the model and avoid falling into the overfitting problem. The genetic algorithm optimizes the initial weights and biases through the global search ability, which overcomes the limitation that the traditional BP neural network is easy to fall into the local optimum, thus reducing the over-fitting of the model to the training data. The selection function is the geometric selection of the norm, the mutation function is the uncombined mutation and the hybridization function is the two-point hybridization with an initial population size of 10 and a maximum evolutionary program of 50. The GA chromosome has 25 genes (weight $4 \times 4 + 1 \times 4 = 20$, threshold $4 + 1 = 5$). The optimization process of the genetic algorithm is illustrated in Fig. 14.

Backpropagation neural network prediction

There were two sets of experimental data used in the GA-BP-ANN model: a training set and a validation set⁴⁵. The model is constructed and trained in the training group, and its usability is confirmed in the validation group. Fifty sets of simulated data were included in the experimental data. The model is learned and trained using 70% of the dataset, and the set is validated using 30%. In the end, 15 validation samples and 35 training samples were acquired. The GA-BP-ANN training was completed at last.

The fitness value is a crucial measure of chromosomal quality in the iterative GA process. The quality of each member of the chromosomal set is indicated by the fitness value. The neural network represented by each chromosome is trained to determine the fitness value based on the training data. The result is the total of the absolute values of the errors in the prediction of all nodes in the output layer, as indicated in Eq. (23).

$$F_{fit} = |y_1 - f_1| + |y_2 - f_2| + |y_3 - f_3| + \dots + |y_N - f_N| \quad (23)$$

where, N is the number of samples, f_i and y_i the predicted and true values of the explosion volume, $i = 1, 2, 3, \dots, n$.

Figure 15(a) presents the curve for GA-BP-AN. During the iteration process, the overall value decreases as the number of iterations increases, indicating that the genetic algorithm optimization is progressing in the right direction. For methane and hydrogen explosion volume predictions, the average fitness values of the populations

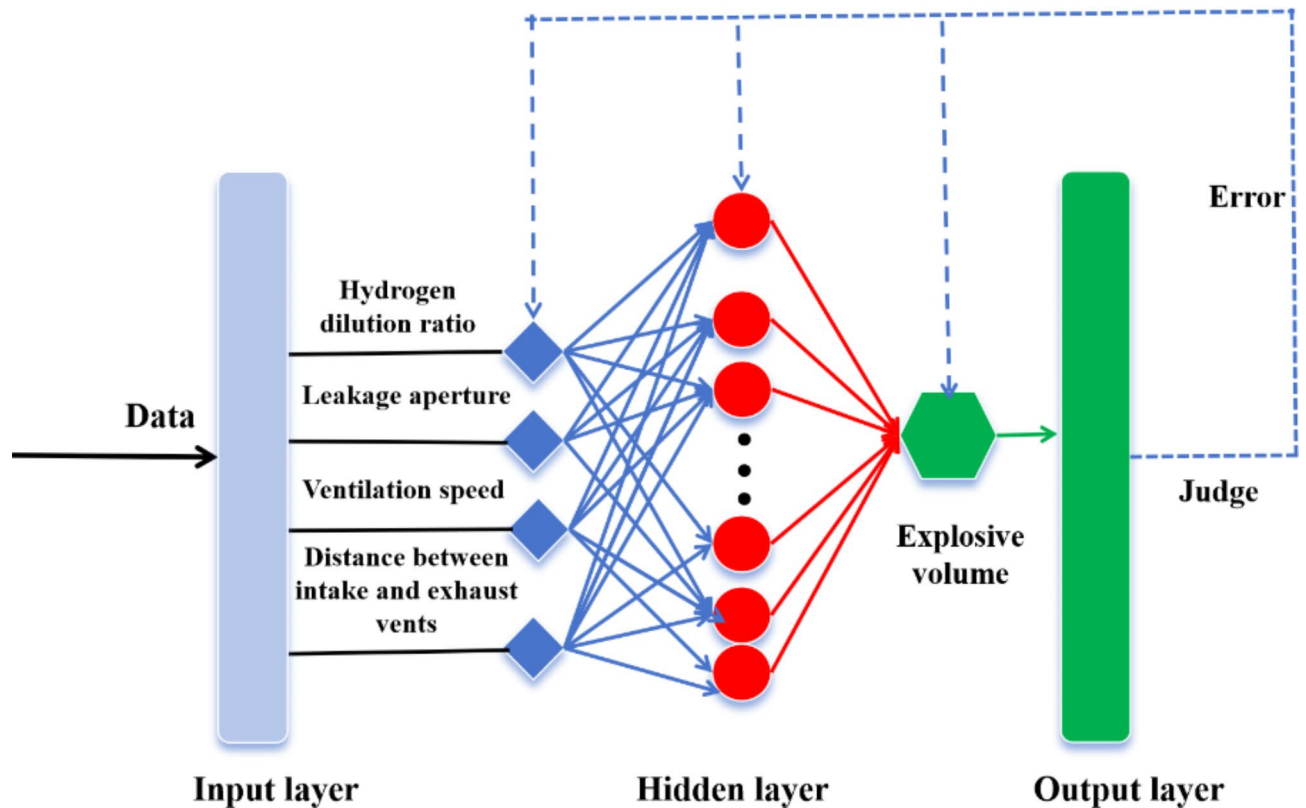


Fig. 13. Neural network topology.

began to stabilize after approximately 30 and 15 iterations, respectively. In the methane group, the weight and threshold of the evolved individuals reached optimal values after 30 iterations, while in the hydrogen group, only 15 iterations were required.

Figure 15(b) and (c) demonstrate how well the training set's actual and projected values match the test set. The constructed GA-BP-ANN model is shown to have strong approximation capacity when the correlation coefficient R^2 between the actual output data and the expected data is near 1. Furthermore, the model performance evaluation index may also be determined using the square correlation coefficient (R^2) and the root mean square error (RMSE), and the equations are computed as Eqs. (24) and (25).

$$RMSE = \sqrt{\frac{1}{N} [(f_1 - y_1)^2 + (f_2 - y_2)^2 + (f_3 - y_3)^2 + \dots + (f_N - y_N)^2]} \quad (24)$$

$$R^2 = 1 - \frac{(f_1 - y_1)^2 + (f_2 - y_2)^2 + (f_3 - y_3)^2 + \dots + (f_N - y_N)^2}{(f_1 - \bar{y})^2 + (f_2 - \bar{y})^2 + (f_3 - \bar{y})^2 + \dots + (f_N - \bar{y})^2} \quad (25)$$

Where, \bar{y} is the average true value.

Table 7 displays the findings of a neural network-based prediction of the methane and hydrogen explosion volume. The established GA-BPANN prediction model's viability is confirmed by the training set data's R^2 of 0.84 and 0.91 and the test set data's R^2 of 0.83 and 0.85.

Conclude

This research uses numerical simulation to model the diffusion distribution of hydrogen-doped natural gas in the extensive pipe gallery. Analysis was done on the impacts of various parameters on the hydrogen explosion volume, methane, concentration field distribution, and velocity field distribution of hydrogen-doped natural gas. BPNN was used to establish a prediction model of the explosion volume of methane and hydrogen after diffusion stabilization of hydrogen-doped natural gas under multi-factor coupling. The conclusion is as follows:

(1) The centerline of the hydrogen-doped natural gas jet's jet in the near-field region is greatly influenced by the leakage hole's diameter. As the leakage hole's size increases, the explosion volume of hydrogen rapidly increases while the explosion volume of methane first increases and then decreases. The majority of the hydrogen-doped natural gas is collected at the top of the pipe gallery and beneath the air outlet, and the explosion volume of hydrogen and methane in the pipe gallery increases with the hydrogen blending ratio. The horizontal jet centerline of the hydrogen-doped natural gas is also deflected upward earlier.

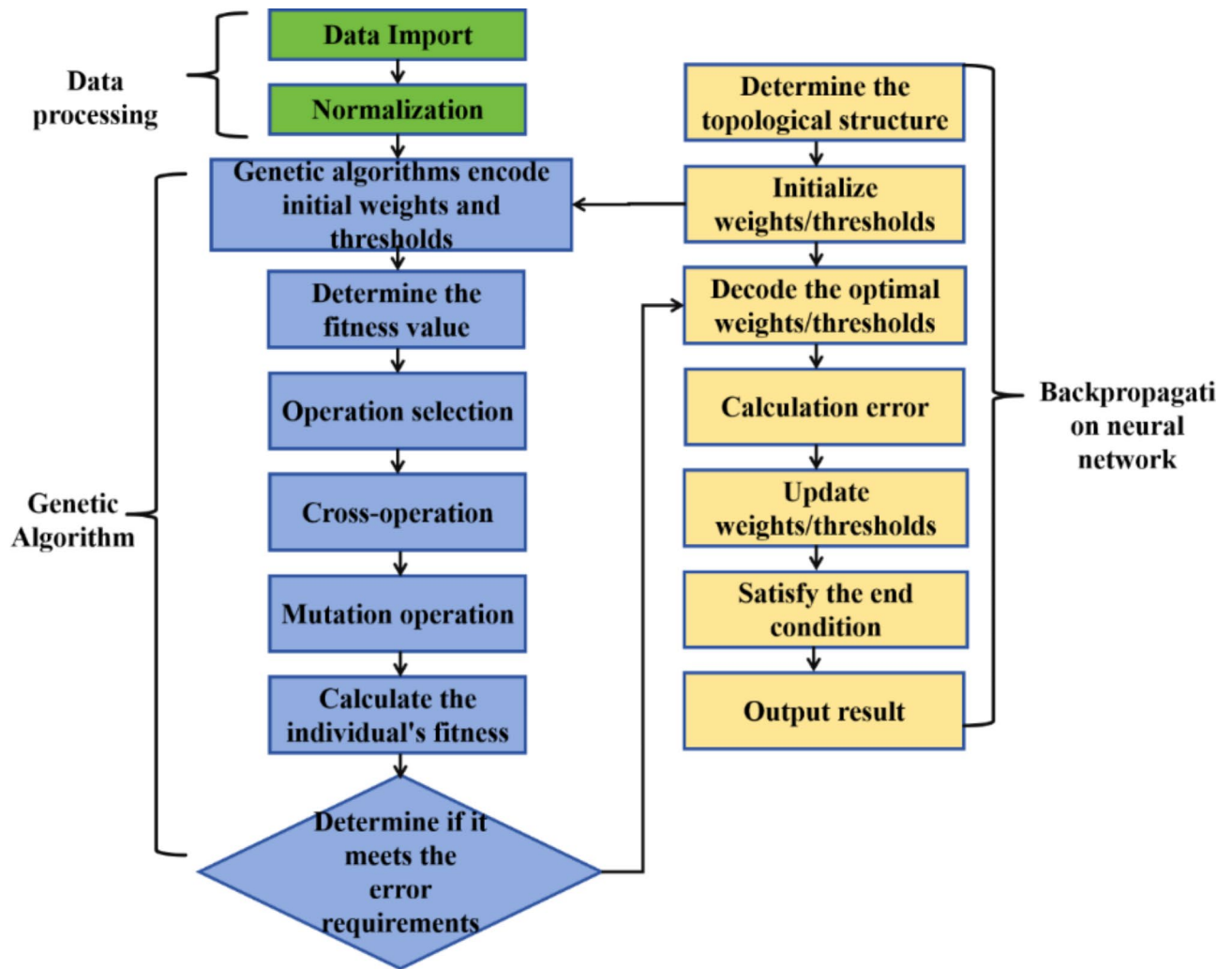


Fig. 14. Genetic algorithm optimization process.

(2) With the increase of wind speed, the gas concentration at the air inlet decreases significantly, and the hydrogen-doped natural gas with high volume fraction no longer gathers above the pipe gallery at the air inlet, and the explosion volume of methane and hydrogen in the pipe gallery decreases. The distance between the air outlet and the leakage point greatly affects the concentration level of hydrogen-doped natural gas in the pipe gallery, and the long-distance air inlet and outlet will lead to the formation of an obvious gas concentration gradient in the pipe gallery, that is, the concentration is higher in the area near the leakage source, and the concentration may be lower in the area far away from the air outlet.

(3) A GA-BPNN surrogate model that can be used to predict the dangerous explosion volume of methane and hydrogen was established. The R^2 of the training set data and the R^2 of the test set data are 0.83 and 0.85, respectively, which verifies the accuracy of the surrogate model.

(4) According to the results of the study, reasonable design of Distance between inlet and outlet and air flow configuration can help to quickly discharge harmful gases and ensure safe evacuation and equipment maintenance in the pipe gallery in an emergency. Therefore, in the design of pipeline infrastructure, for important facilities or high-risk areas, a reasonable mixing ratio of hydrogen should be designed and ensured within the safety threshold of pipeline operation. Moreover, the spacing and wind speed of the inlet and outlet of the pipe corridor should be optimized so that the air can be evenly distributed in the pipe corridor to prevent the accumulation of gas in local areas, so as to effectively reduce the risk of explosion.

(5) Future studies can conduct field experiments in different regions and different types of pipe corridors to collect actual data to validate the simulation model and provide a basis for further optimization of the design. Sensor technology can also be combined with artificial intelligence (such as deep learning) to develop real-time gas concentration monitoring and explosion risk warning systems to improve the safety of pipe corridors.

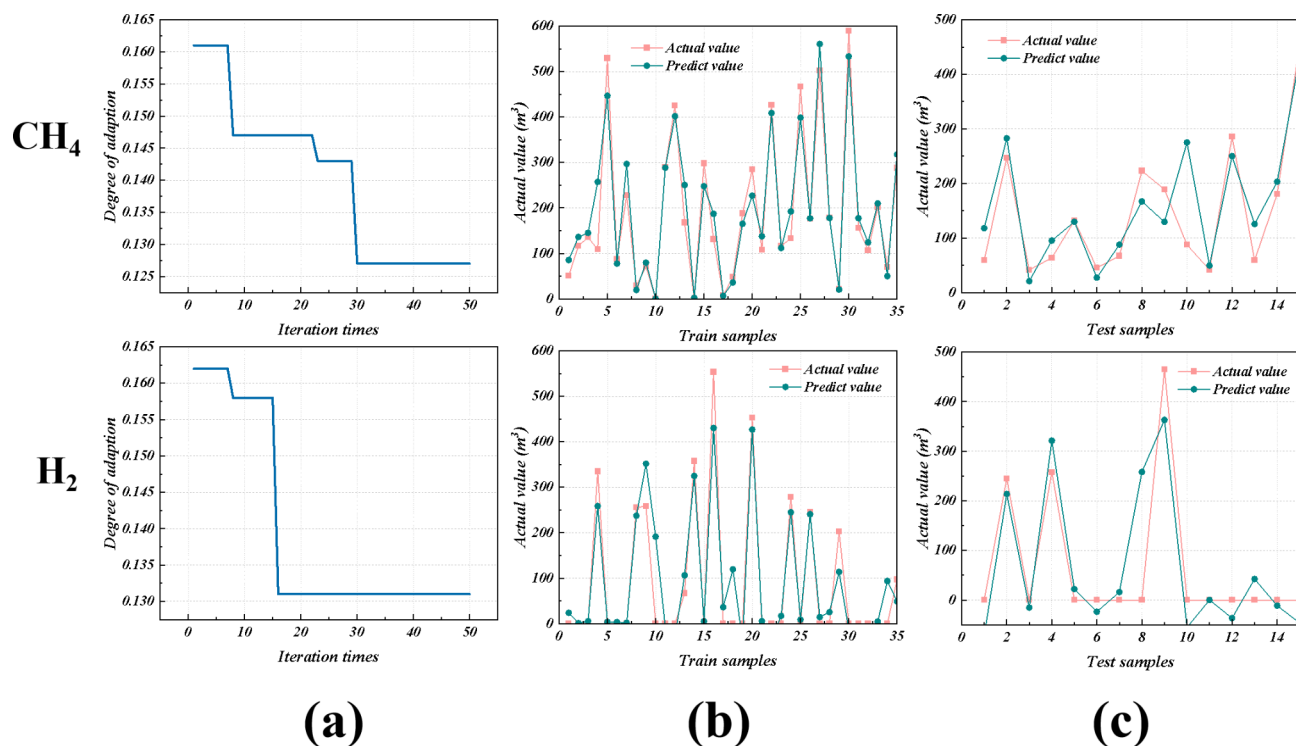


Fig. 15. Neural network prediction results: (a) F_{fit} curve (b) fitting of the actual and predicted values of the train set (c) fitting of the actual and predicted values of the test set.

Prediction type	Train set R^2	Test set R^2
Methane explosion volume	0.84	0.83
Hydrogen explosion volume	0.91	0.85

Table 7. Prediction model data.

Data availability

The data can be provided by the corresponding author if needed.

Received: 5 November 2024; Accepted: 15 January 2025

Published online: 22 January 2025

References

- Field, R. A. & Derwent, R. G. Global warming consequences of replacing natural gas with hydrogen in the domestic energy sectors of future low-carbon economies in the United Kingdom and the United States of America. *Int. J. Hydrog. Energy*. **46** (58), 30190–30203. <https://doi.org/10.1016/j.ijhydene.2021.06.120> (2021).
- Galyas, A. B. et al. Effect of hydrogen blending on the energy capacity of natural gas transmission networks. *Int. J. Hydrog. Energy*. **48** (39), 14795–14807. <https://doi.org/10.1016/j.ijhydene.2022.12.198> (2023).
- JIA, G. W. et al. Hydrogen embrittlement in hydrogen-blended natural gas transportation systems: a review. *Int. J. Hydrog. Energy*. **48** (82), 32137–32157. [10.1016/j.ijhydene.2023.04.266](https://doi.org/10.1016/j.ijhydene.2023.04.266) (2023).
- Shen, X. B., Xiu, G. L. & Wu, S. Z. Experimental study on the explosion characteristics of methane/air mixtures with hydrogen addition. *Appl. Therm. Eng.* **120**, 741–747. <https://doi.org/10.1016/j.applthermaleng.2017.04.040> (2017).
- Askar, E., Schröder, V., Schütz, S. & Seemann, A. Power-to-gas: safety characteristics of hydrogen/natural gas mixtures. *Chem. Eng. Trans.* **48**, 397–402. <https://doi.org/10.3303/CET1648067> (2016).
- Lowesmith, B. J., Hankinson, G., Spataru, C. & Stobbart, M. Gas build-up in a domestic property following releases of methane/hydrogen mixtures. *International Journal of Hydrogen Energy*. **34**(14), 5932–5939. (2009). <https://doi.org/10.1016/j.ijhydene.2009.06.060> (2009).
- Wilkening, H. & Barald, D. CFD modeling of accidental hydrogen release from pipelines. *Int. J. Hydrog. Energy*. **32** (13), 2206–2215. <https://doi.org/10.1016/j.ijhydene.2007.04.022> (2007).
- Li, D. Evaluation of explosion consequence of leakage of hydrogen-doped natural gas in typical confined space. *Chongqing University*. (2021). <https://doi.org/10.13608/j.cnki.1000-4416.2022.05.017>
- Li, R. R., Liu, Z. Y. & Li, P. L. Simulation of indoor hydrogen-doped natural gas leakage stratification. *China Work Saf. Sci. Technol.* **19** (09), 129–135. <https://doi.org/10.11731/j.issn.1673-193x.2023.09.019> (2023).
- Jia, W. L. et al. Study on valve chamber leakage and diffusion law of hydrogen-doped natural gas transmission pipeline. *Oil Gas New Energy*. **33** (06), 75–82. <https://doi.org/10.3969/j.issn.2097-0021.2021.05.014> (2021).

11. De Stefano, M., Rocourt, X., Sochet, I. & Daudey, N. Hydrogen dispersion in a closed environment. *Int. J. Hydrog. Energy*. **44** (17), 9031–9040. <https://doi.org/10.1016/j.ijhydene.2018.06.099> (2019).
12. Mohammad, A. H. A., Saeid, K. & Hossein, S. Numerical study of the effect of hydrogen leakage position and direction on hydrogen distribution in a closed enclosure. *Int. J. Hydrog. Energy*. **45**, 23872–23881. <https://doi.org/10.1016/j.ijhydene.2020.06.202> (2020).
13. Gupta, S., Brinster, J., Studer, E. & Tkatschenko Hydrogen related risks within a private garage: concentration measurements in a realistic full-scale experimental facility. *Int. J. Hydrog. Energy*. **34** (14), 5902–5911. <https://doi.org/10.1016/j.ijhydene.2009.03.026> (2009).
14. Jiang, H. et al. Numerical investigation and analysis of indoor gas explosion: a case study of 6-13 major gas explosion accident in Hubei Province, China. *J. Loss Prev. Process Ind.* **83**, 105045. <https://doi.org/10.1016/j.jlp.2023.105045> (2023).
15. Lei, P. et al. Simulation analysis of the influence of leakage orientation in pipeline corridor on leakage diffusion of natural gas pipeline. *China Work Saf. Sci. Technol.* **17** (10), 133–139. <https://doi.org/10.11731/j.issn.1673-193x.2021.10.020> (2017).
16. Zhou, N. et al. Numerical simulation of the effect of wind speed on leakage and diffusion of natural gas pipe tank in integrated pipeline corridor. *Natural Gas Chemical Industry (C1 Chemistry & Chemical Industry)*. **45**(02),100–105 + 120, (2019).
17. Duan, P. F. et al. Leakage and diffusion characteristics of hydrogen-doped natural gas in pipeline corridors. *Oil Gas Storage Transp.* **42** (8), 901–909. <https://doi.org/10.6047/j.issn.1000-8241.2023.08.006> (2023).
18. Duan, P. F., Chang, X. W., Li, L. L., Liu, J. H. & Li, Y. X. Leakage and alarm response of hydrogen-doped natural gas in pipeline corridors. *Chemical Engineering*. **51**(08), 84–88, (2023). <https://doi.org/10.3969/j.issn.1005-9954.08.016> (2023).
19. Sun, H., Tang, C., Zhou, N., Li, X. & Yuan, X. J. Effect of pipeline pressure on gas leakage and diffusion in natural gas tank of integrated pipeline corridor. *Industrial Saf. Environ. Prot.* **47** (10), 31–34. <https://doi.org/10.3969/j.issn.1001-425X.2021.10.008> (2017).
20. Li, J. T., Qi, C. Z., Chen, H. X., Wang, H. N. & Jin, T. W. Study on effect of slope of integrated pipeline corridor on gas leakage and diffusion. *Fire Sci. Technol.* **40** (01), 42–46 (2021).
21. Zhang, C. et al. Leakage safety analysis of hydrogen-doped natural gas in integrated pipeline corridor. *J. Xi'an Jiaotong Univ.* **58** (02), 22–30. <https://doi.org/10.7652/xjtxb202402003> (2024).
22. Deng, X. J., Yao, A. L., Xu, T. L. & Jiang, H. Y. Study on the law of gas pipeline leakage and diffusion in gas cabin of urban integrated pipeline Corridor. *China Work Saf. Sci. Technol.* **15** (11), 84–89. <http://dx.doi.org/10.11731/j.issn.1673-193x.2019.11.013> (2019).
23. Liu, A. H. et al. Numerical simulation and experiment on the law of urban natural gas leakage and diffusion for different building layouts. *J. Nat. Gas Sci. Eng.* **54**, 1–10. <https://doi.org/10.1016/j.jngse.2018.03.006> (2018).
24. Horvat, A. CFD methodology for simulation of LNG spills and rapid phase transition (RPT). *Process. Saf. Environ. Protection: Trans. Institution Chem. Eng. Part. B.* **120**, 358–369. <https://doi.org/10.1016/j.psep.2018.09.025> (2018).
25. Luo, T. P. et al. Numerical simulation of LNG release and dispersion using a multiphase CFD model. *J. Loss Prev. Process Ind.* **56**, 316–327. <https://doi.org/10.1016/j.jlp.2018.08.001> (2018).
26. Choi, J. et al. A CFD simulation of hydrogen dispersion for the hydrogen leakage from a fuel cell vehicle in an underground parking garage. *Int. J. Hydrog. Energy*. **38** (19), 8084–8091. <https://doi.org/10.1016/j.ijhydene.2013.02.018> (2013).
27. Liu, Y. L. et al. Numerical simulation on the diffusion of hydrogen due to high pressured storage tanks failure. *Loss Prev. Process.* **22** (3), 265–270. <https://doi.org/10.1016/j.jlp.2008.06.007> (2009).
28. Su, Y. Q., Shi, J. F. & Wang, Y. H. Numerical simulation of cavitation of water jet nozzle based on realizable k-ε model. *Mechanics* **28** (1), 12–18. <https://doi.org/10.5755/j02.mech.28583> (2022).
29. Liu, M. Y. et al. A cell-based smoothed finite element model for the analysis of turbulent flow using realizable k-ε model and mixed meshes. *Journal of Computational Physics*. **501**, 112783, (2024). <https://doi.org/10.1016/j.jcp.2024.112783>.
30. Bholu, K. & Shantanu, S. Modelling 2-D supersonic jet from a convergent-divergent nozzle using k-ε realizable turbulence Mode. *J. Phys. Conf. Ser.* **1240** (1), 012019. <https://doi.org/10.1088/1742-6596/1240/1/012019> (2019).
31. Shaheed, R., Mohammadian, A., Kheirkhah, G. & Hossein A comparison of standard k-ε and realizable k-ε turbulence models in curved and confluent channels. *Environ. Fluid Mech.* **19**, 543–568. <https://doi.org/10.1007/s10652-018-9637-1> (2019).
32. GB 50838 – 2015. Technical Specification for Urban Integrated Utility Tunnel Engineering[S].
33. Li, J. F., Su, Y., Zhang, H. & Yu, B. Research progress on the transportation of hydrogen-blended natural gas pipelines. *Nat. Gas. Ind.* **41** (04), 137–152. <https://doi.org/10.3787/j.issn.1000-0976.2021.04.015> (2021).
34. Helena, M., Juan, A. V., Joaquim, C. & Josep, A. Mathematical modelling of accidental gas releases. *J. Hazard. Mater.* **59** (2), 211–233. [https://doi.org/10.1016/S0304-3894\(97\)00149-0](https://doi.org/10.1016/S0304-3894(97)00149-0) (1998).
35. Shao, X. Y. et al. Study on the difference of dispersion behavior between hydrogen and methane in utility tunnel. *Int. J. Hydrog. Energy*. **47** (12), 8130–8144. <https://doi.org/10.1016/j.ijhydene.2021.12.123> (2022).
36. Yan, X. K., Wang, L. J. & Chen, Y. H. FLUENT Chemical Fluid Computation and Application Examples. *Xuzhou: China University of Mining and Technology Press*, (2022).
37. Grubb, J. W. Simplifying CFD modeling of longwall gobs with a modular meshing approach. *Indian Heart J.* **67** (3), 68–72. <https://doi.org/10.1155/2010/472636> (2015).
38. Chi, M. et al. The erosion rate prediction for the elbow in shale gas gathering and transportation system: RSM and GA-BP-ANN modeling. *Powder Technol.* **435**, 119–429. <https://doi.org/10.1016/j.powtec.2024.119429> (2024).
39. Zhang, H. T., Li, X. R. & Kong, T. Application of BP neural network in missing data estimation. *Comput. Eng. Des.* **14**, 3457–3459. <https://doi.org/10.16208/j.issn1000-7024.2007.14.055> (2007).
40. Zhang, H. & Tian, Z. G. Failure analysis of corroded high-strength pipeline subject to hydrogen damage based on FEM and GA-BP neural network. *Int. J. Hydrog. Energy*. **47** (7), 4741–4758. <https://doi.org/10.1016/j.ijhydene.2021.11.082> (2022).
41. Li, Y. J., Wang, Z. R. & Shang, Z. Analysis and prediction of hydrogen-blended natural gas diffusion from various pipeline leakage sources based on CFD and ANN approach. *Int. J. Hydrog. Energy*. **53**, 535–549. <https://doi.org/10.1016/j.ijhydene.2023.12.018> (2024).
42. Huang, F. C., Liu, D. X., An, T. S. & Cao, J. Port Container Throughput Forecast Based on ABC Optimized BP Neural Network. *IOP Conference Series: Earth and Environmental Science*, **571**, 012068. (2020). <https://doi.org/10.1088/1755-1315/571/1/012068>
43. Zhang, J. F., Wang, L., Liu, M. & Wang, S. Prediction of surface roughness errors based on improved genetic algorithm optimized BP neural network. *J. High. Educ. Sci.* **43** (07), 33–40. <https://doi.org/10.3969/j.issn.1007-9831.2023.07.008> (2023).
44. Li, B. et al. Factor analysis and GA-BP-ANN prediction of nitrogen diffusion behavior in underground laboratory under ventilation conditions. *Sci. Rep.* **14** (1), 1–22. <https://doi.org/10.1038/s41598-024-63829-8> (2024).
45. Yan, W., Wang, Z. R., Ouyang, D. X. & Chen, S. C. Analysis and prediction of thermal runaway propagation interval in confined space based on response surface methodology and artificial neural network. *J. Energy Storage*. **55**, 105822. <https://doi.org/10.1016/j.est.2022.105822> (2022).

Author contributions

Xiaolong Gong: Conceptualization, Investigation, Methodology, Software, Visualization, Writing—original draft, Writing—review & editing. Hua li: Conceptualization, Methodology, Resources, Supervision. Cheng li: Formal analysis, Investigation. Mingyue kou: Formal analysis, Investigation. Lingxu kong: Formal analysis, Investigation, Methodology. Hongcheng liu: Formal analysis, Investigation.

Declarations

Competing interests

The authors declare no competing interests.

Additional information

Correspondence and requests for materials should be addressed to M.K.

Reprints and permissions information is available at www.nature.com/reprints.

Publisher's note Springer Nature remains neutral with regard to jurisdictional claims in published maps and institutional affiliations.

Open Access This article is licensed under a Creative Commons Attribution-NonCommercial-NoDerivatives 4.0 International License, which permits any non-commercial use, sharing, distribution and reproduction in any medium or format, as long as you give appropriate credit to the original author(s) and the source, provide a link to the Creative Commons licence, and indicate if you modified the licensed material. You do not have permission under this licence to share adapted material derived from this article or parts of it. The images or other third party material in this article are included in the article's Creative Commons licence, unless indicated otherwise in a credit line to the material. If material is not included in the article's Creative Commons licence and your intended use is not permitted by statutory regulation or exceeds the permitted use, you will need to obtain permission directly from the copyright holder. To view a copy of this licence, visit <http://creativecommons.org/licenses/by-nc-nd/4.0/>.

© The Author(s) 2025